Remote Sensing of Environment 188 (2017) 9–25

Contents lists available at ScienceDirect

Remote Sensing of Environment

journal homepage: www.elsevier.com/locate/rse

Toward mapping crop progress at field scales through fusion of Landsat and MODIS imagery

Feng Gao [a,*], Martha C. Anderson [a], Xiaoyang Zhang [b], Zhengwei Yang [c], Joseph G. Alfieri [a], William P. Kustas [a], Rick Mueller [c], David M. Johnson [c], John H. Prueger [d]

[a] USDA, Agricultural Research Service, Hydrology and Remote Sensing Laboratory, 10300 Baltimore Avenue, Beltsville, MD 20705, USA
[b] Geospatial Sciences Center of Excellence and Department of Geography, South Dakota State University, Brookings, SD 57007, USA
[c] USDA, National Agricultural Statistics Service, 3251 Old Lee Highway, Fairfax, VA 22030, USA
[d] USDA, Agricultural Research Service, National Laboratory for Agriculture and the Environment, Ames, IA 50011, USA

ARTICLE INFO

Article history:
Received 4 December 2015
Received in revised form 28 October 2016
Accepted 3 November 2016
Available online 10 November 2016

Keywords:
Crop growth stages
Phenology
Crop conditions
Crop progress
Crop yield
Data fusion
Time-series analysis

ABSTRACT

The ability to regionally monitor crop progress and condition through the growing season benefits both crop management and yield estimation. In the United States, these metrics are reported weekly at state or district (multiple counties) levels by the U.S. Department of Agriculture (USDA) National Agricultural Statistics Service (NASS) using field observations provided by trained local reporters. However, the ground data collection process supporting this effort is time consuming and subjective. Furthermore, operational crop management and yield estimation efforts require information with more granularity than at the state or district level. This paper evaluates remote sensing approaches for mapping crop phenology using vegetation index time-series generated by fusing Landsat and MODIS (Moderate Resolution Imaging Spectroradiometer) surface reflectance imagery to improve temporal sampling over that provided by Landsat alone. The case study focuses on an agricultural region in central Iowa from 2001 to 2014. Our objectives are 1) to assess Landsat-MODIS data fusion results over cropland; 2) to map crop phenology at 30 m resolution using fused surface reflectance data; and 3) to identify the relationships between remotely sensed crop phenology metrics and the crop progress stages reported by NASS. The results show that detailed spatial and temporal variability in vegetation development across this landscape can be identified using the fused Landsat-MODIS data. The mean difference (bias) in Normalized Difference Vegetation Index (NDVI) between actual Landsat observations and the fused Landsat-MODIS data, generated for Landsat overpass dates, is in the range of −0.011 to 0.028 for every year. The derived phenological metrics show distinct features for different crops and natural vegetation at field scales. Strong correlations are observed between remotely sensed phenological stages, based on NDVI curve inflection points, and the observed crop physiological growth stages from the NASS Crop Progress (CP) reports. The green-up dates detected from remote sensing data typically occurred during crop vegetative stages when 2–4 leaves were developed for both corn and soybeans, or about 1–3 weeks after the reported emergence dates when the plant were first visible to ground-based observers. Despite being a lagging indicator, remotely sensed green-up can be used effectively to backcast emergence, e.g. as input to spatially distributed crop models. The differences in green-up date between corn and soybean were 8–10 days, consistent with the offset in emergence dates reported by NASS at district level. The reported harvest dates were typically about 2–3 weeks after the dormancy stage was detected via remote sensing for corn and about 1–2 weeks for soybeans. This suggests that probable harvest times for individual fields may be predicted 1–3 weeks ahead using remote sensing data. The results suggest that crop phenology and certain growth stages at field scales (30 m spatial resolution) can be linked and mapped by integrating imagery from multiple remote sensing platforms.

Published by Elsevier Inc.

1. Introduction

Accurate spatiotemporal information about crop progress and condition during the growing season is critical for crop management and yield estimation (Walthall et al., 2012; Sakamoto et al., 2013). The amount of yield loss realized during a drought year is dependent on the crop growth stage when water stress occurs. For this reason, irrigation applications may be modulated depending on crop growth stage. Crop progress provides information necessary for efficient irrigation and drainage management. For example, the most beneficial timing for irrigation is during the latter part of the reproductive growth stages

* Corresponding author.
E-mail address: feng.gao@ars.usda.gov (F. Gao).

http://dx.doi.org/10.1016/j.rse.2016.11.004
0034-4257/Published by Elsevier Inc.

for soybeans versus the earlier tasseling period for corn. In addition, crop progress information is critical for scheduling fertilization, pest management and harvesting operations at optimal times for achieving higher yields. For food security and commodity trading, it is vital to estimate crop yield before harvest. Crop progress and growth condition data sets provide information that is needed for yield estimation.

Crop progress varies by year and location and is affected by climate variation, local weather, soil properties, environmental changes and anthropogenic activities. Over the past three decades, both corn and soybean in the U.S. have been planted increasingly earlier in the spring. Corn planting dates have advanced by 10 days and soybean by 12 days from 1981 to 2005 (Kucharik, 2006; Walthall et al., 2012). This earlier planting has been accompanied by a longer growing season, both of which contribute to yield increases. These trends can also be observed from U.S. Department of Agriculture (USDA) National Agricultural Statistics Service (NASS) publications on the planting and harvesting dates for field crops (NASS Field Crops, 1997, 2010). In addition to climate and local weather variation, crop phenology trends also reflect changing farm management strategies and development of new cold-hardy genotypes (Kucharik, 2006). High spatial resolution information about relative changes in characteristic phenology due to varying climate and anthropogenic activities are important for understanding vegetation responses to climate variation, and for facilitating better decision making to mitigate drought impacts and to support adaptation strategies.

In the United States, crop progress and condition are estimated by USDA NASS using ground survey data supplied by ~4000 reporters. These reporters provide visual observations and subjective estimates of crop progress based on NASS standard definitions. Crop growth stages, crop conditions and farmers' activities are reported each week. The NASS Crop Progress (CP) reports are summarized and released weekly during the growing season from early April to late November (NASS CPR, 2015). Weekly CP reports are among the most requested publications released by NASS and have substantial impacts for future crop market prices (Lehecka, 2014). Even though the weekly reports have been carefully checked for data consistency, the ground data collection is time consuming and subjective. The quality of crop progress and condition assessments depends on the individual reporter's experience and subjective judgment. The report provides the public with summaries at the agricultural statistic district (multiple counties) and state level. These reports do not discuss spatial variability within the agricultural statistical unit. For many applications such as precision agricultural management, mapping crop phenology at field scale is required.

Remote sensing data can be an effective supplement to ground-based observation, providing spatial and temporal information for vegetation monitoring over large areas. In recent years, time-series of coarse resolution data, such as from the Advanced Very High Resolution Radiometer (AVHRR) and the Moderate-resolution Imaging Spectroradiometer (MODIS), have been used to extract vegetation phenology (Reed et al., 1994; Zhang et al., 2003; Jonsson and Eklundh, 2004; Zhao et al., 2009, 2012). These approaches use mathematical functions to fit time-series of vegetation indices (VIs). Vegetation phenology or phenological parameters are extracted based on either a predefined VI threshold (Reed et al., 1994; Jonsson and Eklundh, 2004) or the inflection points of the fitting function (Zhang et al., 2003). Using 4 years of time-series AVHRR NDVI data, Reed et al. (1994) generated 12 phenological metrics including the onset of greenness, time of peak NDVI, maximum NDVI, rate of green-up, rate of senescence, and integrated area under the curve. Jonsson and Eklundh (2004) developed a software tool (TIMESAT) to analyze time-series VI data based on three fitting approaches (asymmetric Gaussians, double logistic function, and Savitzky-Golay filter). Eleven phenological parameters are extracted based on the fitting functions and the pre-defined threshold. Zhang et al. (2003) and Zhang (2015) developed a phenology program using a hybrid piecewise logistic function and the approach has been used to produce the MODIS phenology data product since 2001. All these approaches extract vegetation phenology using particular features in time-series VI data, which can be interpreted as remote sensing phenology. In order to relate phenology detected from remote sensing signals to the field observed crop progress (or physiological stages), Sakamoto et al. (2010, 2011) developed a two-step filtering approach to detect maize and soybean phenology using MODIS data. In their approach, a shape-model of Wide Dynamic Range Vegetation Index (WDRVI) was defined for each crop. The shape-model serves as a priori information to fit observed MODIS WDRVI data. The phenological stages were computed (or modified from a priori) based on the fitting parameters. The approach was applied to map crop progress in the U.S. Corn Belt using MODIS data (Sakamoto et al., 2011) and to estimate corn grain yield at the state level (Sakamoto et al., 2013). Zhao et al. (2012) assessed the impact of the temporal resolution of the input image timeseries on the accuracy of the remote sensing based phenology estimation. These studies reveal that dense time-series remote sensing data provide better temporal information for mapping vegetation phenology at coarse spatial resolution.

Global land cover and land surface phenology products are available at 500 m MODIS spatial resolution (Friedl et al., 2002; Zhang et al., 2003). However, the 500 m spatial resolution is still too coarse for many crop fields. It often represents mixtures of vegetation or crop types which may have very different phenological growth cycles. Crop phenology is most appropriately investigated at field scales, well-supported in the United States by the Landsat spatial resolution in the reflectance bands (30 m). Spatial details at this resolution can be well captured in land cover and land use classification (Loveland and Dwyer, 2012; Roy et al., 2014). The USDA NASS produces the Cropland Data Layer (CDL) in the United States annually at 30-m resolution (Boryan et al., 2011) using a combination of Landsat, Disaster Monitoring Constellation UK-2 and Deimos-1 imagery (NASS CDL, 2015). It would be ideal to have crop progress information at the same spatial resolution for crop management and yield estimation. However, Landsat and medium-resolution satellite imagery are normally acquired over a narrow swath and thus the revisiting cycles are relatively long (from a few days to over 20 days). The lack of frequent medium-resolution data is a major barrier to mapping crop phenology and progress at field scales.

Landsat data have been freely available since 2008 (Woodcock et al., 2008). Landsat 5 was launched on March 1, 1984. The Thematic Mapper (TM) instrument aboard Landsat 5 provided 30-m resolution data for over 28 years until 2012. Landsat 7 was launched on April 15, 1999, carrying the Enhanced Thematic Mapper (ETM+). Despite the failure of the scan-line-corrector (SLC) which causes data gaps in the ETM+ imagery, Landsat 7 is still providing useful information over about 80% of a given Landsat scene. Landsat 8 was launched on February 11, 2013. The Operational Land Imager (OLI) instrument aboard Landsat 8 provides high quality 30-m resolution shortwave data on a 16 day repeat cycle. The Landsat TM, ETM+ and OLI data have been processed to surface reflectance using a MODIS-like atmospheric correction approach (Vermote et al., 2002; Masek et al., 2006) and can be downloaded from the US Geological Survey (USGS) Earth Resources Observation Systems (EROS) data center. The recently launched Multispectral Imager on Sentinel-2A mission by European Space Agency has a global acquisition plan and the data products will be freely available. The effective revisit cycle could be shortened to a few days if Landsat and Sentinel-2 data sets are combined.

Until more frequent Landsat-resolution imagery becomes available, data fusion techniques provide a solution for bridging between Landsat observations using high temporal resolution MODIS data collected at somewhat coarser spatial scales. This data fusion approach (Gao et al., 2006; Hilker et al., 2009; Zhu et al., 2010) combines the spatial resolution of Landsat with the temporal frequency of MODIS and thus provides a feasible and economic solution for integrating remote sensing data from different satellite sources. The Spatial and Temporal Adaptive Reflectance Fusion Model (STARFM) uses comparisons of one or more

pairs of observed Landsat/MODIS maps, collected on the same day, to predict maps at Landsat-scale on other MODIS observation dates (Gao et al., 2006, 2015). STARFM was subsequently modified and extended for different applications to form the Spatial Temporal Adaptive Algorithm for mapping Reflectance Change (STAARCH) for detecting reflectance changes associated with land cover change and disturbance (Hilker et al., 2009), and an enhanced STARFM (ESTARFM) approach developed to handle more heterogeneous scenes, where "pure" pixels are lacking (Zhu et al., 2010). Walker et al. (2012) used the STARFM data fusion approach to generate synthetic imagery for tracking phenological changes over a dryland vegetation site in Arizona. Liang et al. (2014) compared the land surface phenology derived from MODIS and the fused Landsat-MODIS data to ground measurements and found that the fused Landsat-MODIS data can better capture land surface phenology at the community level (0.1–20 ha) in a northern U.S. mixed forest than using MODIS alone.

Here we extend the application of data fusion down to sub-field scales for phenology mapping over agricultural landscapes. The main objective of this paper is to test the ability of this Landsat-MODIS data fusion methodology to map crop phenology at 30-m resolution, where crop growth stages for different crops can be distinguished. Specifically this paper aims: 1) to generate and evaluate the fused Landsat-MODIS daily surface reflectance and the derived NDVI at 30-m resolution over an intensively cropped area; 2) to map crop phenology at 30 m resolution (sub-field scale) using the fused Landsat-MODIS data; and 3) to identify the relationships between crop phenology detected from remote sensing data and the crop progress stages reported by NASS. Our study focuses on an agricultural area in central Iowa, USA from 2001 to 2014.

2. Study area and data preparation

2.1. Study area

Fig. 1 shows the study area in central Iowa overlaid with the Landsat scene (path 26 and row 31). This is a rain-fed agricultural area in the U.S. Corn Belt region. Corn and soybean are the major cover types, and these crops are typically rotated in consecutive years. Major natural vegetation types include deciduous forest and grasslands. There are also small portions of developed surfaces (roads and buildings) in the area. The Landsat scene covers the South Fork watershed (subset window), and includes a USDA Agricultural Research Service (ARS) Long Term Agricultural Research (LTAR) site instrumented with micrometeorological flux towers. This study site is located in the middle of the U.S. Corn Belt and rain-fed Corn Belt area.

2.2. Crop progress reports

USDA NASS publishes weekly Crop Progress (CP) reports quantifying the cumulative progress for major crops at the key growth stages in terms of percentages. The key physiological growth stages are defined by NASS as shown in Table 1 (extracted from the NASS Terms, 2015).

District-level crop progress reports from 2010 to 2014 were obtained from the NASS public website (NASS CPR, 2015). Data for the "central

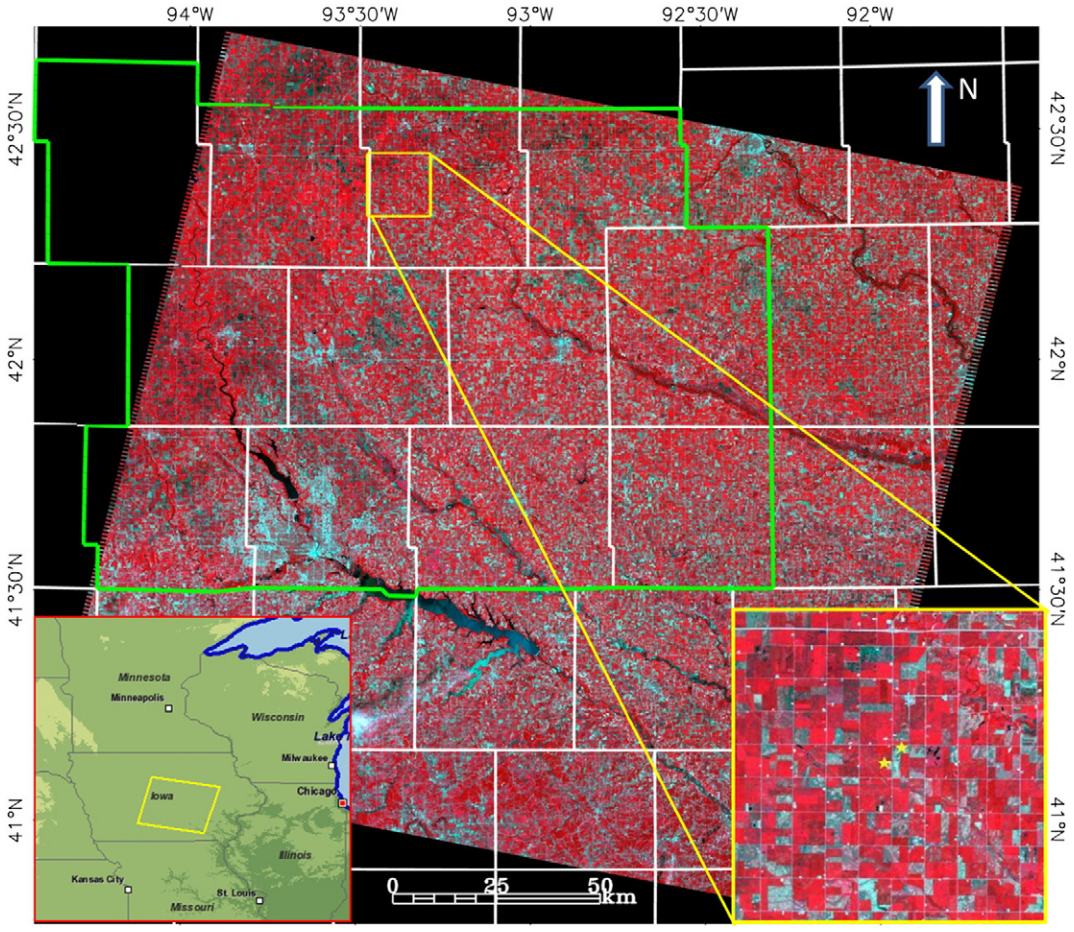

Fig. 1. Landsat scene (path 26 and row 31) containing the research area (central Iowa, yellow polygon in lower left map) overlaid with county boundaries (white lines), agricultural district boundaries (central Iowa, green polygon), and two flux tower sites (yellow stars in lower right image). The subset area in the lower right was chosen to demonstrate results for better visualization.

Table 1
Key growing stages and descriptions for corn and soybeans from NASS.

Corn	Definition	Soybeans	Definition	Phenology from remote sensing
Emerged	As soon as the plants are visible	Emerged	As soon as the plants are visible	Green-up
Silking	The emergence of silk-like strands from the end of ears	Blooming	A plant should be considered as blooming as soon as one bloom appears.	Mid-season
Dough	Normally half of the kernels are showing dent with some thick or dough-like substance in all kernels	Setting pods	Pods are developing on the lower nodes with some blooming still occurring on the upper nodes	Mid-season
Dent	Occurs when all kernels are fully dented and the ear is firm and solid			Mid-season
Mature	Plant is considered safe from frost. Corn is about ready to harvest with shucks opening and there is no green foliage present	Dropping leaves	Leaves near the bottom of the plant are yellow and dropping, while leaves at the very top may still be green. Leaves are 30–50% yellow	Dormancy
Harvest		Harvest		Dormancy

Iowa" district (green polygon in Fig. 1) were extracted, mainly coinciding with the processed Landsat scene (p26r31). In addition, county-level crop progress data for 2010 and 2011 for 17 counties completely covered by the Landsat scene were obtained directly from NASS under a signed confidentiality agreement, and were quality controlled for obvious data entry errors. These data are proprietary; therefore, to maintain the confidentiality of the raw data and the observation locations, the associated county name and actual ID Numbers are not revealed in this study. For these reasons, the analyses in this paper mainly rely on the published district level data.

2.3. Landsat and MODIS data

Nine years of Landsat and MODIS data from 2001 to 2014 were chosen to generate the fused Landsat-MODIS reflectance time-series for crop phenology mapping. Fig. 2 shows Landsat dates for the selected years that were used in the study, including all clear and partially clear Landsat 5, 7, and 8 images. All Landsat images were evaluated visually, and the cloud mask distributed with the Landsat surface reflectance data products (Zhu and Woodcock, 2012, 2015) was consulted to eliminate use of cloudy pixels/scenes in the data fusion and phenology processes. Only mostly clear Landsat scenes (dots in time axis for each year) were used as fine resolution images to pair with MODIS data as input to STARFM. Partially clear Landsat images (dots below the time axis for each year) were not used in the data fusion process. Landsat 7 images (yellow dots) that suffer SLC failure after May 2003 were not used as input pair images since SLC-off gaps will remain in the fused images and affect the subsequent phenology mapping. However, all valid and clear pixels (as identified in the cloud mask) from all available Landsat images, including partially clear and Landsat 7 SLC-off images, were used in the phenology mapping itself. From 2001 to 2011, Landsat 5 TM (red dots) and Landsat 7 ETM+ data were used. For 2013 and 2014, Landsat 7 ETM+ and Landsat 8 OLI (green dots) data were used. The vertical lines bracket prediction periods where a given Landsat-MODIS image pair was used as input to the data fusion process. The period for data fusion using that pair was determined using the maximum correlation criteria as described later in Section 3.1.

The required MODIS data products for the selected years from 2001 to 2014 were ordered and processed. These include the daily surface reflectance at both 250 m (MOD09GQ) and 500 m (MOD09GA) resolution (Vermote et al., 2002), the MODIS Bidirectional Reflectance Distribution Function (BRDF) parameters at 500 m resolution (MCD43A1; Schaaf et al., 2002, 2011), and the MODIS land cover types at 500 m resolution (MCD12Q1; Friedl et al., 2002). In order to cover the entire Landsat scene (path 26 and row 31), two MODIS tiles (h10v04 and h11v04) were ordered and mosaicked. MODIS Collection 5 data products were used in this study.

Selection of years used in the analyses (Fig. 2) was governed by data availability. For 2010–2014, when NASS CP reports for central Iowa (district level) were available for assessment, all years were processed except 2012. In 2012, Landsat 5 TM reached the end of its serviceable life and only MSS data were collected in the study area, while Landsat 7 ETM+ images suffer SLC-off gaps. The only available Landsat images for 2012 are the Landsat 7 SLC-off ETM+ images. For this reason, 2012 was not processed and analyzed. Prior to 2010, every 1–3 years were sampled for analysis of inter-annual variations. In these earlier years, NASS CP reports are only available at the state level, and ground

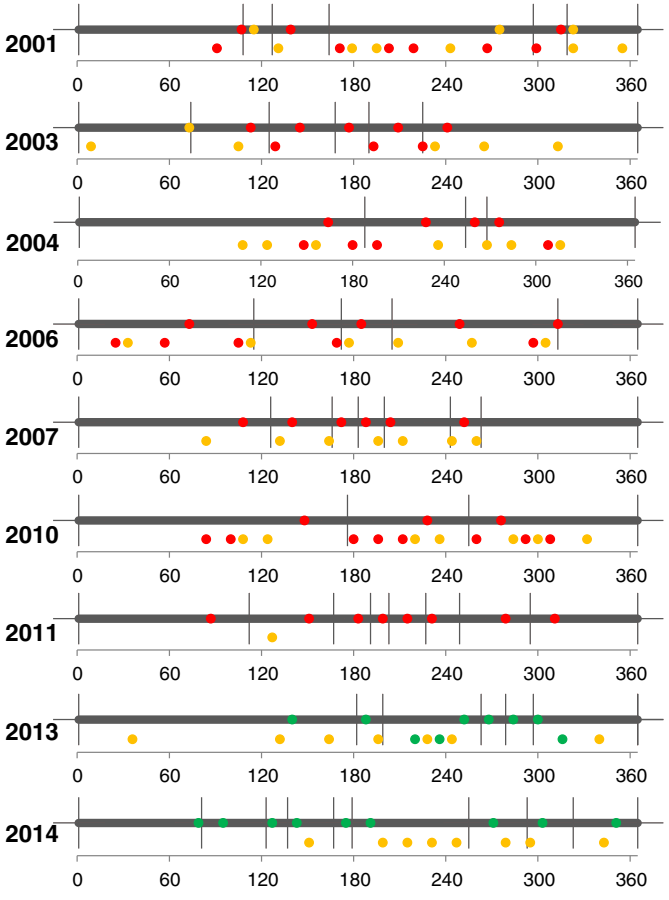

Fig. 2. Landsat images from 2001 to 2014 that were used in data fusion and crop phenology mapping. Each dot represents a Landsat acquisition, while the vertical lines bracket prediction periods where a given Landsat-MODIS image pair was used as input to the data fusion process. Dots within the time (x) axis indicate Landsat images that were used as pair images in the data fusion process; dots below the time axis represent Landsat images that were not used in data fusion but used in phenology mapping. Red, yellow, and green dots represent Landsat 5 TM (2001—2011), Landsat 7 ETM+ and Landsat 8 OLI respectively.

observations and flux tower measurements were not available. Still, these earlier years allow us to investigate the inter-annual variation of crop phenology over a wider time range.

2.4. Cropland Data Layer (CDL)

The Cropland Data Layer provides crop type information at field scales (Boryan et al., 2011). NASS CDL 30-m resolution data from 2001 to 2014 were downloaded and used to analyze the crop phenology patterns for major crop types over the study area. CDL products prior to 2006 were generated based on Landsat 5/7 imagery. From 2006 to 2008, imagery from other satellites/sensors including the Advanced Wide Field Sensor (AWiFS) on IRS-P6 and MODIS NDVI on Terra were used in the CDL production. The CDL products were derived using Landsat imagery from 2008 and 2009. The CDL program used the Disaster Monitoring Constellation (DMC) satellites (i.e., Deimos-1 and UK-2) and Landsat 5/7 imagery since 2011 and Landsat 8 OLI imagery since 2013. In Iowa from 2001 to 2014, the overall classification accuracies for major crops (soybeans and corn) are generally above 96%, except for 2001 (92–95%). Soybean and corn crops were normally rotated in two consecutive years although there are some variations due to the implementation of new bioenergy policies (Ren et al., 2014). All CDL data were reprojected and resampled to match the Landsat scene (path 26 and row 31).

2.5. Flux tower data

In-situ meteorological and surface flux measurements were collected over a pair of adjacent agricultural fields north of Ames (near Buckeye), IA in Hardin County. The fields are nominally 800 m by 800 m in size and characterized by flat terrain and clay loam soils. They are managed following a maize/soybean rotation strategy, with the crop type alternating between the two fields on an annual basis.

The micrometeorological system deployed in each field was equipped with a sonic anemometer (CSAT3, Campbell Scientific Inc., Logan, Utah[1]) to measure the orthogonal wind velocity components and an open-path infrared gas analyzer (LI-7500, Li-COR Biosciences, Lincoln, Nebraska) to measure both water vapor and carbon dioxide concentration. The flux data were post-processed using the full complement of standard corrections and adjustments. Nonphysical values and outliers were removed without replacement from the high -frequency (20 Hz) data using a moving window algorithm based on the method outlined by Goring and Nikora (2002). The half-hourly corrected fluxes were used to generate the daily mean data used in this analysis. The gross primary production (GPP) for the corn and soybean sites was derived from the measured daytime net ecosystem exchange (NEE) and the daytime ecosystem respiration (RE) estimated using regression equations between nighttime NEE and soil temperature (Xiao et al., 2004). We chose a simple empirical approach to estimate GPP since our objective is to examine the temporal trends of NEE/GPP in comparison to time-series NDVI during different crop growth stages. More accurate partitioning approaches need to include additional meteorological forcing variables and may consider ecosystem model inversion techniques.

2.6. Field biophysical data

Field observations of crop progress were conducted during growing seasons from 2010 to 2013, sampling two observation sites in Dallas County, Iowa located within the study area. The observation sites were at least 300 yards (274 m) away from other crop fields, major roads, buildings, and rivers etc. The observation fields selected were at least 50 acres (0.202 km^2) in size with a regular shape (not elongated or concave) so that the fields cover sufficient pure image pixels. Each site was located inside a single homogenous crop field (either corn or soybean) representing field conditions and farm practices typical for the region. Fifteen plants each for corn and soybeans were systematically selected at geolocated sites within the fields following specific documented procedures. The vegetative crop growth progress stages of every selected corn and soybeans plants were observed and recorded weekly at fields by enumerators after planting. The height of each plant was measured and recorded every week. The overall crop growth stage for each crop was determined by the majority growing stage observed. Photographs of every sampled plant were acquired with a GPS enabled digital camera for quality control and validation. Observations from these two sites were compared to phenological metrics retrieved in the associated Landsat pixels.

3. Methods

The analyses conducted in this study include two core components: data fusion and phenology extraction. The entire processing flow chart is shown in Fig. 3, and briefly summarized here. In the data fusion process, MODIS daily directional surface reflectance products are corrected to daily Nadir BRDF-adjusted Reflectance (NBAR). In this study, the Landsat Digital Numbers (DN) were calibrated and atmospherically corrected using the Landsat Ecosystem Disturbance Adaptive Processing System (LEDAPS) (Masek et al., 2006). The Landsat surface reflectance can also be directly ordered and downloaded from the USGS EROS data center. Landsat and MODIS reflectances in the red and near infrared bands are then fused using the STARFM approach (Gao et al., 2006). The phenology extraction process was applied to NDVI timeseries generated using both the fused Landsat-MODIS surface reflectances and the observed reflectances acquired directly on Landsat days. Crop phenological dates and metrics extracted from remote sensing data were assessed in comparison with carbon flux measurements, field observations, and crop progress statistics obtained from NASS CP reports at both the county level (under a signed confidentiality agreement) and

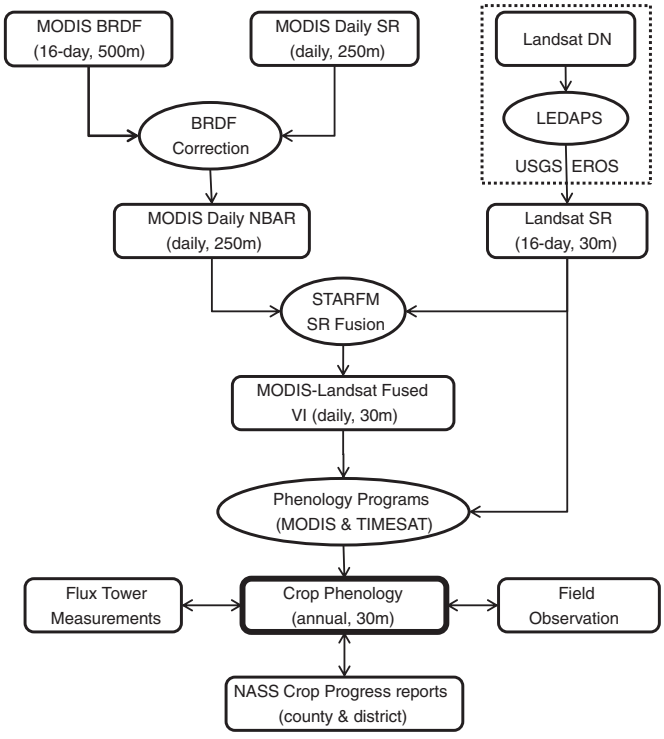

Fig. 3. Crop phenology data processing and analysis flow chart (rectangles indicate data products and ellipses represent processing steps/modules).

[1] Mention of trade names or commercial products in this article is solely for the purpose of providing specific information and does not imply recommendation or endorsement by the U.S. Department of Agriculture.

the district level (from the public web site). Key techniques and methods are described below.

3.1. Landsat-MODIS data fusion

The STARFM data fusion approach has been described in detail in Gao et al. (2006). An operational data fusion system has been developed to process MODIS and Landsat surface reflectance data semi-automatically (Wang et al., 2014). This system implemented several procedures to improve computational efficiency (Gao et al., 2015), consistency between Landsat and MODIS inputs, and to automate selection of an optimal Landsat-MODIS input pair for each prediction date. Some issues of relevance to routine phenology mapping are discussed in further detail in this section.

3.1.1. Data consistency between Landsat and MODIS

The data fusion algorithm requires that input data from the sensors to be fused are reasonably consistent, i.e., data products from Landsat and MODIS should be highly correlated and comparable in both time and space so that the temporal and spatial variability from two data sources can be reasonably combined. We have chosen to fuse Landsat and MODIS surface reflectance products rather than derived vegetation indices because STARFM requires that the coarse resolution image can be linearly aggregated from a fine resolution image.

Prior to fusion, corrections are applied to the input imagery to maximize consistency and usability of Landsat-MODIS image pairs. Normalization of the MODIS daily directional surface reflectance to Nadir BRDF-adjusted Reflectance (NBAR) improves correlations with Landsat imagery, which are collected at near-nadir view angles (Gao et al., 2010; Feng et al., 2013). More precise co-registration of the MODIS and Landsat pair images is achieved through a pixel-incremented shift procedure that maximizes spatial correlation.

After these corrections, it is useful to assess the consistency between input imagery used in a fusion experiment. This information can be valuable in interpreting unexpected behavior and apparent biases in the output timeseries. In this study, Landsat 5 TM, Landsat 7 ETM +, and Landsat 8 OLI surface reflectance were used. Landsat TM/ETM + and MODIS surface reflectance has been examined in previous studies (Gao et al., 2006; Feng et al., 2013). Landsat 8 OLI bandwidths are slightly different from TM and ETM, which can lead to biases with respect to MODIS. To conduct the assessment, the Landsat and MODIS surface reflectances were first resampled to 960 m spatial resolution for pixel-to-pixel comparison. An aggregate resolution, coarser than the native resolution of the MODIS reflectance products, was used in this comparison to reduce the effects of varying MODIS pixel footprint size with different view angles (Tan et al., 2006). For off-nadir views, the MODIS pixel becomes increasing elongated, and may encompass a different set of Landsat pixels depending on the view angle. Cloud masks from Landsat and MODIS surface reflectance products were used to exclude cloudy pixels. The remaining clear Landsat and MODIS pixels acquired from the same day were used to generate the statistics.

In addition, the fused Landsat-MODIS output surface reflectances and the derived NDVI were compared to actual Landsat observations that were not used in data fusion due to clouds or gaps. Only clear pixels from these actual Landsat observations were used for comparison at Landsat 30 m resolution.

3.1.2. Selection of Landsat-MODIS input pairs

The STARFM algorithm can use one or two input pairs of Landsat and MODIS images to predict a Landsat-like image on a MODIS date where a Landsat overpass is not available. In this study, we used the single-pair option because in a highly dynamic agricultural Midwestern landscape it is difficult to obtain two clear Landsat-MODIS image pairs with surface conditions reasonably similar to the target retrieval date. Furthermore, variations in MODIS pixel footprint with viewing angle can further degrade consistency between input and retrieval dates even under stable surface conditions.

For the single-pair option, the fusion package has two automated approaches for assigning an input MODIS-Landsat image pair to each prediction date within the targeted output timeframe. The two automatic options in the system include 1) choosing the image pair with the nearest date to the prediction date, or 2) using the image pair that has the highest spatial correlation with the MODIS image on the prediction date. In practice, spatial correlation coefficients are computed for MODIS images on all possible pair (Landsat overpass) and prediction dates. Then for each prediction date, the pair with the highest correlation is saved in pair selection table used in the fusion process. In general, this tends to produce similar results to option (1), but the temporal bounds of reconstruction governed by a given input image pair may shift somewhat based on rates of change in land-surface conditions. The temporal bounds developed through automated option (2) in this study are indicated as vertical bars in Fig. 2.

3.2. Extracting phenology at field scale

The final output NDVI time-series from the data fusion system combines the actual Landsat observations on Landsat overpass dates and the fused Landsat-MODIS data retrieved between Landsat overpasses. The phenology extraction process employed here used all clear pixels, identified using the Landsat cloud mask, from all available Landsat observations deemed either clear or partially clear.

Two established phenology approaches (TIMESAT and MODIS) were evaluated for both utility and ease of implementation. The TIMESAT program (Jonsson and Eklundh, 2004) provides eleven phenological metrics, including dates of start of growing season and end of growing season. The TIMESAT software smoothes the NDVI data and fits them to a selected function, using either asymmetric Gaussians, double logistic or Savitzky-Golay filters. The key phenological metrics - start and end of the season - are identified as dates when the NDVI passes predefined thresholds, defined in terms of percentage of the seasonal amplitude (maximum value minus minimum base value) in the NDVI. These thresholds need to be appropriately defined to capture the growth stages.

The MODIS phenology algorithm (Zhang et al., 2003) uses a piecewise logistic fitting function. Time-series features that indicate the onset of green-up, the onset of maturity, the onset of senescence, and the onset of dormancy are determined by the curvature of the logistic function. The curvature of a smooth function measures how quickly a curve is changing at a given point. The curvature approach does not require any pre-defined thresholds. For comparison to TIMESAT phenological metrics and crop growth stages, only green-up dates (start of the season) and dormancy dates (end of the season) were extracted in this study.

Both phenology approaches work better when more than one year of time-series data are available. In our study area, crop rotation is a common practice and farmers normally plant different crops (i.e. soybeans or corn) in two consecutive years. Including multiple years of remote sensing data may introduce uncertainties due to land cover changes. In order to generate crop phenology for a specific year (referred to as the "focus year"), we have extended each focus year of VI data to two years by padding with data from the same year. Data from the first half of the year were added after the end of the focus year, while data from the second half of the year were inserted before the beginning of the focus year. The padded time-series were only used for constructing time-series functions. Only dates within the focus year were used to determine phenology dates and phenological metrics.

The fitting functions in both phenology programs allow differential weighting of time-series data at a given pixel. In this study, we assigned three classes of weights at the pixel level to represent different data sources and quality. For the observed Landsat data, clear pixels were weighted as 1.0 (full contribution) while cloudy or missing pixels

(e.g., due to the SLC failure on Landsat 7) were assigned as 0.0 (no contribution). For the fused Landsat-MODIS data, the weights for the valid pixels were assigned as 0.25 (reduced contribution). These weights were empirical estimates based on the data quality and previous assessment (Gao et al., 2008). The MODIS phenology approach was modified to use the same data smoothing and filtering preprocessing as used in the TIMESAT program. Other information, such as land surface temperature used in the MODIS phenology program, was not used in this study. These modifications were made to maximize similarity in inputs to both programs, and to better focus on evaluating the two phenology approaches themselves (threshold vs. curvature).

3.3. Linking remote sensing phenology to crop growth stages

Crop phenology extracted from remote sensing data is an indirect estimate of physiological crop growth stages, and is based on seasonal variations in greenness. To relate to crop growth stages, crop phenology metrics obtained from the remote sensing data were assessed using ground observations made in-field (Section 2.6) and as summarized at the county and district levels in the NASS crop progress reports (Section 2.2). Crop progress reports average planting, fruiting, and harvesting progress for crops within the reporting district. For corn, progress on the percentages of crops planted, emerged, tasseled, silked, milk, doughing, dented, mature, and harvested are reported weekly (NASS Terms, 2015). For soybean, weekly progress on the percentage of crops planted, emerged, bloomed, setting pods, turning colour, dropping leaves, and harvested are reported (Table 1). Since remote sensing phenology dates are directly related to changes of crop greenness, this research focuses on retrieval of the growth stages that are most sensitive to remote sensing observations, such as the green-up and dormancy dates. The green-up (or start of the season) dates were compared to the reported crop emergence dates. The dormancy (or end of the season) dates were compared to the mature dates (or leaf-dropping stage for soybean) and harvest dates. Comparisons were conducted for corn and soybeans separately. The median dates of green-up and dormancy for each county and for the "central Iowa" district were extracted and compared to the median dates of crop growth stages from the NASS crop progress reports. In addition, as a spot check on general reasonability of the fused NDVI time-series reconstruction, we compared retrieved NDVI with NEE/GPP curves derived from flux measurements at the tower sites described in Section 2.5. Qualitative agreement in timing between these independent measures of crop productivity adds some additional confidence that the fusion is providing reasonable temporal information.

4. Results and analysis

The data fusion results and crop phenology were analyzed using the entire Landsat scene (path 26 and row 31), which covers central Iowa. Some results are demonstrated for the subset area (Fig. 1) around South Fork, Iowa for better visualization.

4.1. Landsat-MODIS fusion results

4.1.1. Input data consistency between Landsat and MODIS

As mentioned above, the level of consistency between Landsat and MODIS reflectance inputs can affect the accuracy of the data fusion results. Therefore, assessment of temporal and intra-sensor biases can provide valuable information for interpreting performance in the output time series. Using the 960-m aggregated reflectance datasets described in Section 3.1.1, the differences between Landsat and MODIS daily NBAR on average over all years for the study site were within ± 0.012 for the red band and within ± 0.025 for the NIR band. The mean absolute differences were <0.015 and 0.030 for the red and NIR bands, respectively. The R^2 for all years were above 0.73 for the red band and above 0.86 for the NIR band.

Although Landsat shows good agreement with MODIS surface reflectance products, the agreement varies among Landsat sensors due to differences in sensor characteristics (e.g. sensor bandwidths, band response functions), satellite orbit (e.g. solar and viewing angles), and data processing approach (e.g. calibration and atmospheric correction). Landsat-7 ETM + surface reflectances show small biases and mean absolute differences, as well as higher R^2, in comparison with Terra MODIS data. This is likely because the Landsat 7 and Terra satellites are in the same orbit, and the overlap swath is collected at similar view angles, near nadir. Furthermore, MODIS geolocation accuracy is best at nadir view. The newer Landsat-8 OLI sensor has a narrow bandwidth in the NIR, similar to that on MODIS, giving significantly smaller mean differences between OLI and MODIS for the NIR band in 2013 and 2014 in comparison with ETM +. However, OLI-MODIS mean absolute differences (MAD) were larger and R^2 were smaller, and this was likely due to view angle effects. The MODIS observations on the Landsat 5 and 8 acquisition dates were mostly collected from off-nadir viewing angles. Even though the angular effect on BRDF has been corrected in this study, the footprint of a given MODIS pixel is much larger at a large off-nadir view (Tan et al., 2006). The aggregated Landsat and MODIS pixels at off-nadir view may not match exactly. In addition, differences in aerosol information used in the Landsat and MODIS atmospheric corrections may introduce some dissimilarity in the resulting surface reflectance products (Vermote et al., 2002; Masek et al., 2006).

The STARFM data fusion approach takes into account time invariant differences in reflectance between Landsat and MODIS. In theory, a systematic bias between Landsat and MODIS for the prediction period does not affect data fusion results since the STARFM model uses the difference of reflectance in the prediction. However, if biases vary during the prediction period, these variations can affect the fusion results. Fig. 4 shows the variation in bias (Landsat minus MODIS) for the red and NIR bands between pair images for each year. Landsat 8 OLI data are plotted separately for the evaluation. Consistent time-series Landsat-MODIS fusion results can be expected if Landsat and MODIS pair images show consistent biases (flat line) during the year. In Fig. 4, the NIR band shows higher variation in bias than the red band especially during growing season, which may be due to the higher reflectance in the NIR band during the growing season. Landsat-8 OLI data in 2014 show smaller variations in bias during the growing season. More reliable fusion results for OLI surface reflectances can be expected in this case. Note that even though Landsat 5 and 7 reflectances for most years were consistently higher in the red band and lower in the NIR band, these systematic biases will not affect the STARFM fusion results. Only the time variation in these biases will be problematic.

4.1.2. Assessment of fused Landsat-MODIS reflectance

Nine years of the fused Landsat-MODIS surface reflectances at 30 m resolution were generated for central Iowa. The accuracy of the Landsat-scale reflectance predictions at 30-m resolution was assessed by comparing fused Landsat-MODIS reflectances and actual Landsat observations that were not used in the data fusion process (observations plotted below the horizontal lines in Fig. 2). These Landsat images include partially cloudy scenes and ETM + images affected by the SLC failure. All cloudy and invalid pixels were excluded from comparison. Table 2 shows statistics from this inter-comparison, using all unused Landsat images available in a given year as the basis for comparison. The mean biases were within ± 0.01 for the red band and within ± 0.02 for the NIR band. The 2007 and 2011 show higher negative biases (-0.008 and -0.004) in the red band, which are due in part to the large variation in biases between Landsat and MODIS pair images for these two years (Fig. 4a). Similarly the high positive biases in the NIR band for 2004 and 2006 (0.018 and 0.016) were partially caused by a large temporal variation in MODIS-Landsat bias (Fig. 4b). The root-mean-square difference (RMSD) for 2013 and 2014 between fused and observed NIR band reflectances were slightly higher than for the rest of the years since OLI images were primarily used as pair images while

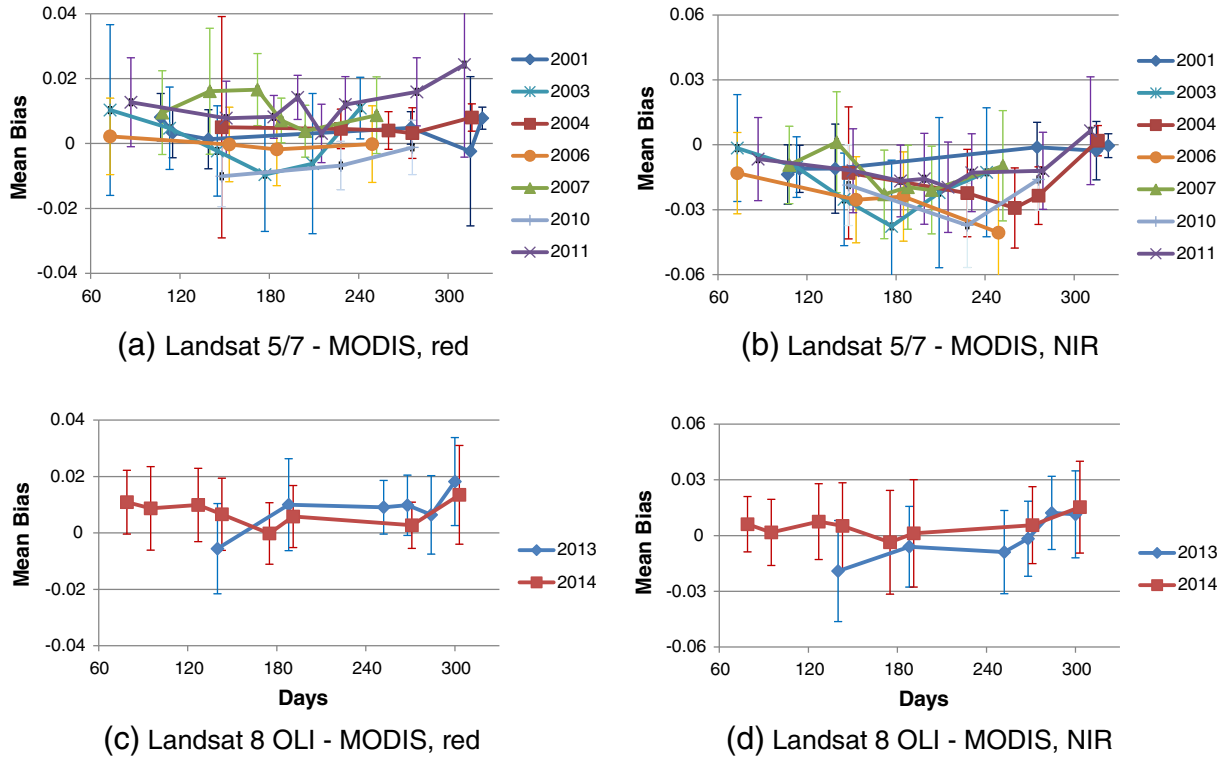

Fig. 4. Mean bias (lines) and standard deviation (bars) between Landsat surface reflectance and MODIS daily NBAR for the red and NIR bands in pair images for each year of the study. A consistent bias through time will not affect fusion results, while variation in bias will.

all ETM + images were used to assess the fusion results. The difference between OLI and ETM + surface reflectance may partially contribute to this higher variation. For all years, the correlations (R^2) between the fused Landsat-MODIS data and actual Landsat observations were above 0.54 and 0.65 for the red and NIR bands, respectively. The mean absolute differences (MAD) were within 0.026 for the red band and 0.053 for the NIR band.

4.1.3. NDVI time-series

Daily NDVI images at 30-m resolution were computed using the fused surface reflectances. Fig. 5 shows a subset of NDVI images extracted every half month from early April to middle October in 2011, along with the CDL classifications for 2011 in the lower right. Clear seasonal trends in NDVI for crops and natural vegetation can be identified at these field scales. Deciduous forest (northeast part of the subset) shows higher NDVI and earlier green-up than do crop pixels. Most of the vegetated pixels reach maximum NDVI in early August. Corn and soybean crops senesce in early to middle October. These fields can be clearly recognized in the early and late growing season, in contrast to the forested pixels.

To compare temporal patterns in the fused datasets at the 30-m pixel level, time-series NDVI were extracted for three representative pixels (corn, soybean, and forest) during the growing season. Both fused Landsat-MODIS data and the observed Landsat data are plotted in Fig. 6 along with the fitting curves using a double logistic function. The corn and soybean samples were selected from the two flux tower sites in South Fork, Iowa, while the forest sample was taken from an area near the tower sites. Each class shows a distinct temporal pattern in NDVI evolution. The forest pixel greens-up early, reaches maximum NDVI in early spring, and shows high NDVI values in September and even in October images. Among the cropped pixels, corn NDVI increases earlier than soybean and both crops reach maximum NDVI in late July to early August. The contrast in NDVI between land cover types is most pronounced during the spring, which suggests that the spring images are more appropriate for land cover and crop type classification if only red and NIR bands are available or used. During the summer, the corn sample shows a longer plateau near maximum NDVI – corn greens up earlier than soybean and senesces later, consistent with a longer growing period. The NDVI for the soybean sample decreased more quickly than the corn and forest samples during the fall.

Similar to the reflectance comparisons discussed in Section 4.1.2, NDVI derived from the fused Landsat-MODIS surface reflectances at 30-m pixel resolution were compared to Landsat data that were not used as input to the data fusion process. Table 3 shows the mean bias, RMSD, mean absolute difference and R^2 for the fused and observed NDVI data at 30-m resolution. Biases in NDVI for all years are in the range of −0.011 to 0.028. All years show high correlations ($R^2 > 0.8$). The mean absolute differences (MAD) in NDVI are <0.083 for all years. The high positive NDVI biases for 2007 and 2011 are due to the larger negative biases in the red band, while the high positive NDVI bias in 2004 is due to the large positive bias in the NIR band (see Table 2).

Table 2
Mean bias (MB), root-mean-square difference (RMSD), mean absolute difference (MAD) and R^2 computed at 30-m resolution between the fused Landsat-MODIS data and actual Landsat observations not used as input to the data fusion due to gaps or clouds (i.e., dots below the horizontal lines in Fig. 2).

	Red				NIR			
Year	MB	RMSD	MAD	R^2	MB	RMSD	MAD	R^2
2001	−0.001	0.024	0.017	0.637	−0.004	0.059	0.044	0.731
2003	−0.003	0.026	0.018	0.674	0.001	0.056	0.037	0.735
2004	0.001	0.030	0.020	0.601	0.018	0.058	0.045	0.739
2006	0.004	0.029	0.020	0.646	0.016	0.052	0.040	0.707
2007	−0.008	0.025	0.017	0.713	−0.003	0.063	0.035	0.702
2010	0.000	0.033	0.022	0.619	−0.003	0.060	0.044	0.656
2011	−0.004	0.023	0.016	0.791	0.008	0.050	0.038	0.769
2013	0.004	0.036	0.026	0.540	0.013	0.063	0.047	0.664
2014	−0.002	0.028	0.019	0.636	0.012	0.073	0.053	0.656

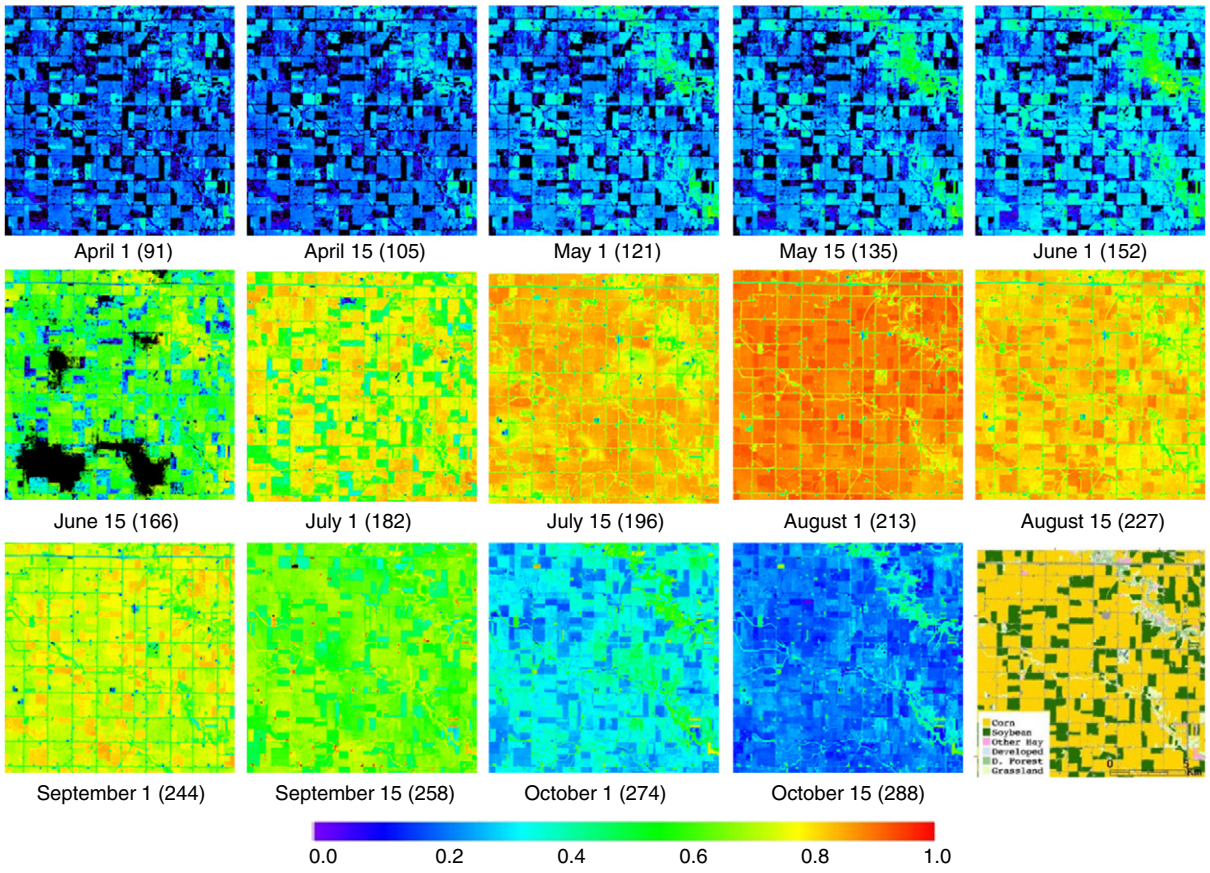

Fig. 5. NDVI time-series computed from the fused Landsat-MODIS surface reflectances for a subset area (South Folk, Iowa) from April 1 to October 15, 2011 (black pixels in the June 15 image are missing values due to cloud contamination in the MODIS image for that day).

4.2. Crop phenology at field scale

4.2.1. Phenology from remote sensing approaches

Two approaches (MODIS and TIMESAT) were applied to extract crop phenology from the daily time-series NDVI. The TIMESAT approach relies on a pre-defined threshold (percent change of the seasonal amplitude between minimum and maximum NDVI values) to determine the start of the season, the end of the season, and the length of the season. The MODIS phenology approach uses curvature analyses to identify inflection points in the fitting curve. In this study, a double logistic function was selected to fit time-series NDVI for both approaches.

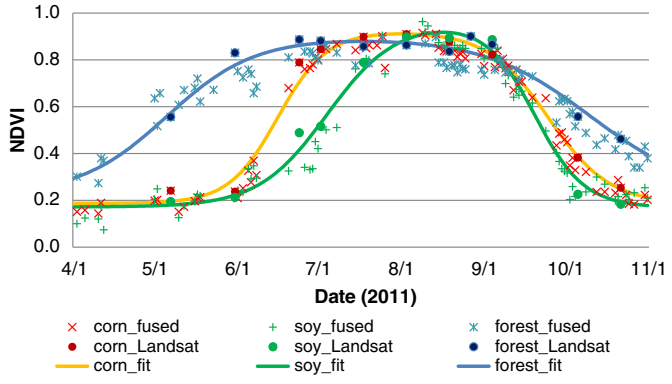

Fig. 6. Corn, soybean and forest (near tower site) pixels show different temporal patterns of NDVI from early April to late October in 2011. Both the fused Landsat-MODIS data and actual Landsat observations (dots) were used to construct fitting curves using a double logistic function (lines).

Fig. 7 shows the green-up dates detected using different thresholds (TIMESAT) and the curvature approach (MODIS) for 2011 and 2014. For comparison with CP report data, which represent cumulative percentages of growth stages, the remote sensing green-up dates (or the start of the season) were also plotted as cumulative percentages generated from the distribution of pixels across the entire Landsat scene. The crop growth stages were extracted from the NASS CP reports at the district level for central Iowa. Reporters observe and report on crop emergence as soon as plants are visible, but this early stage was not detectable from spaceborne observations of NDVI. Therefore, the remotely sensed green-up dates were later than the reported emerged dates.

In Fig. 7, the reported emergence dates for corn are close to the green-up date produced using a 10% threshold in TIMESAT, while the emergence dates for soybean were closer to the predicted dates using a 15% threshold. The TIMESAT program sets the default threshold at

Table 3
Mean bias (MB), root-mean-square difference (RMSD), mean absolute difference (MAD) and R^2 between NDVI derived from the fused Landsat-MODIS reflectance and the actual Landsat observations (not used in data fusion) based on 30-m resolution pixels for each year.

Year	MB	RMSD	MAD	R^2
2001	−0.004	0.098	0.072	0.856
2003	0.010	0.093	0.064	0.879
2004	0.021	0.115	0.083	0.801
2006	0.006	0.108	0.078	0.817
2007	0.027	0.095	0.068	0.815
2010	−0.011	0.107	0.077	0.826
2011	0.028	0.083	0.066	0.896
2013	0.006	0.103	0.077	0.844
2014	0.011	0.097	0.071	0.846

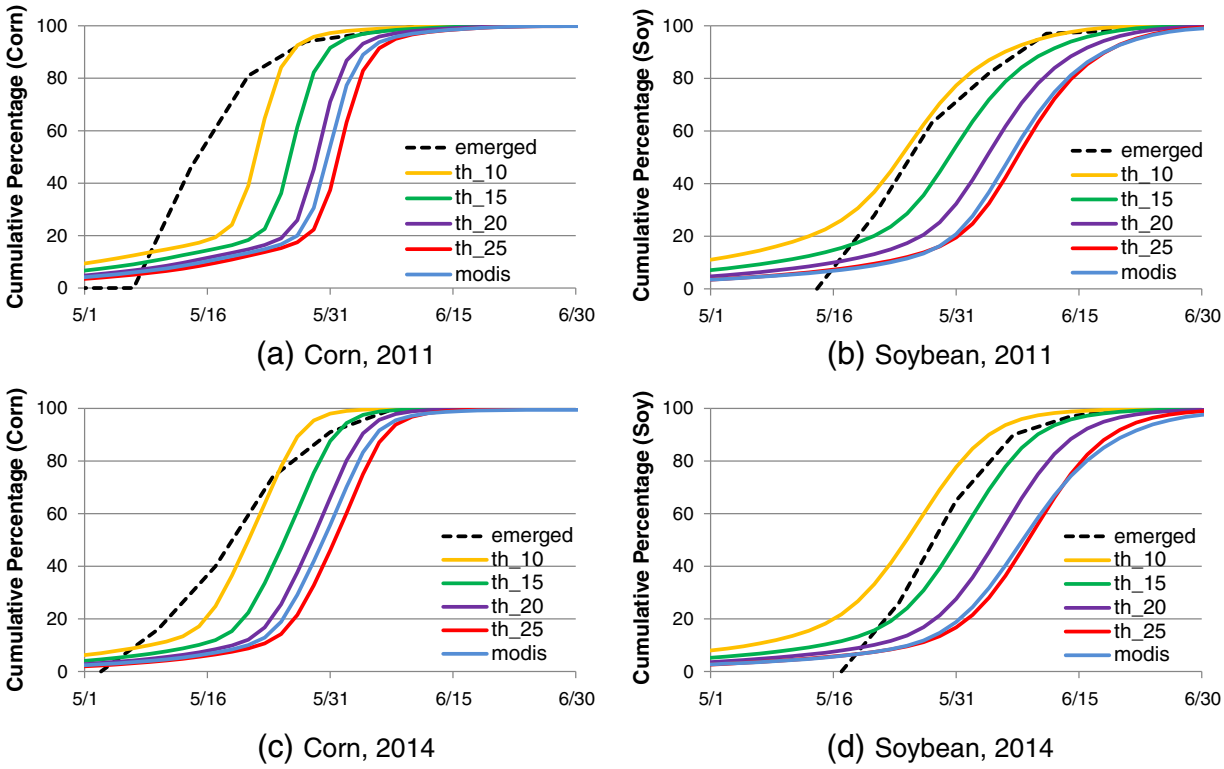

Fig. 7. Green-up (or the start of the season) dates from different phenology approaches and the percent emergence (dashed lines) reported in the CP reports for central Iowa in 2011 and 2014 show different relationships. The MODIS curvature approach (blue lines) predicts later green-up dates than the CP emergence observations, but the differences of green-up dates between corn and soybeans were relatively stable. The TIMESAT threshold approach using different threshold levels (10%, 15%, 20%, and 25%) shows variations in the green-up dates between corn and soybeans.

20%, which produced results close to the MODIS curvature approach in the study area. A smaller threshold can generate earlier green-up dates, but it is also sensitive to noise and small variations in time-series NDVI and thus less reliable. The MODIS curvature approach produces more consistent green-up dates for both corn and soybean.

The best time to plant corn in Iowa, on average, is from late April to early May. Soybeans are usually planted one to two weeks later than corn. As published in the CP reports, 9% of corn in central Iowa was planted by May 1, 2011 and 78% by May 8, 2011, while 14% of soybeans was planted by May 8 and 62% by May 15. In other words, soybeans were planted a week later than corn. The median reported corn emergence dates (at 50% cumulative histogram level) in the CP reports were 9–10 days ahead of soybeans for both 2011 and 2014. The median corn green-up dates were 8–9 days ahead of the soybeans from the MODIS curvature approach, which was consistent with the CP reports. However, the threshold approach produced different results varying from 2 to 10 days at 10%, 15%, 20% and 25% thresholds (th_10, th_15, th_20, and th_25 in Fig. 7). With a 25% threshold, the TIMESAT approach produced similar green-up dates to the MODIS curvature approach for soybeans but later green-up dates for corn. This implies that different thresholds may be needed for different crops in order to compare to the emergence dates in the CP reports. In addition, the green-up dates from TIMESAT also depend on the amplitude between minimum and maximum NDVI values. This requires clear Landsat/MODIS observations around the peak growing season in order to obtain reliable maximum NDVI. From a practical standpoint, the MODIS curvature approach produced more consistent green-up dates for corn and soybeans. This feature is important for building a standard procedure to map crop phenology. The curvature approach does not require a pre-determined threshold and green-up dates only depend on the observations during the early growing season, thereby enhancing utility for realtime applications. The phenology dates were more consistent for corn and soybeans. For these reasons, the MODIS curvature approach is used in the remainder of this paper to map crop phenology and to assess connections with physiological crop growth stages.

4.2.2. Mapping phenology at field scale

Crop phenology detected from remote sensing data provides valuable information about field-to-field spatial variability in crop development over agricultural landscapes. Fig. 8 illustrates green-up and dormancy dates for the selected years from 2001 to 2014, zooming into a subset area in South Fork, Iowa. Corn and soybeans show clearly different green-up dates. For all years, corn showed earlier green-up than soybean as revealed in histograms of green-up dates (second row in Fig. 8). Green-up dates for corn in 2006 were earlier than for the other three years, likely due to the early favorable conditions (warmer than average and dry enough for machinery operation in 2006 around the local area) for seedling development. In 2011, corn green-up dates were distributed over a relatively shorter period of time around early June, with some overlap with green-up time for soybean crops. While variability in dormancy dates between fields is apparent, the differences in dormancy dates were not as obvious as differences in green-up dates between the two crops (see histograms in Fig. 8). In 2006, peak dormancy dates for corn occurred slightly earlier than for soybean, while the opposite relative timing is inferred in 2011. In 2001 and 2014, dormancy dates for the two crops were very close. Forest pixels always showed an earlier green-up date and a later dormancy date, as exemplified by the individual forest sample in Fig. 6.

4.3. Phenology and crop progress stages

Crop phenology metrics retrieved from the fused Landsat-MODIS data were compared to crop growth stages reported at district and county levels from the NASS CP reports. Observations at the field scale were examined using the corresponding Landsat pixels.

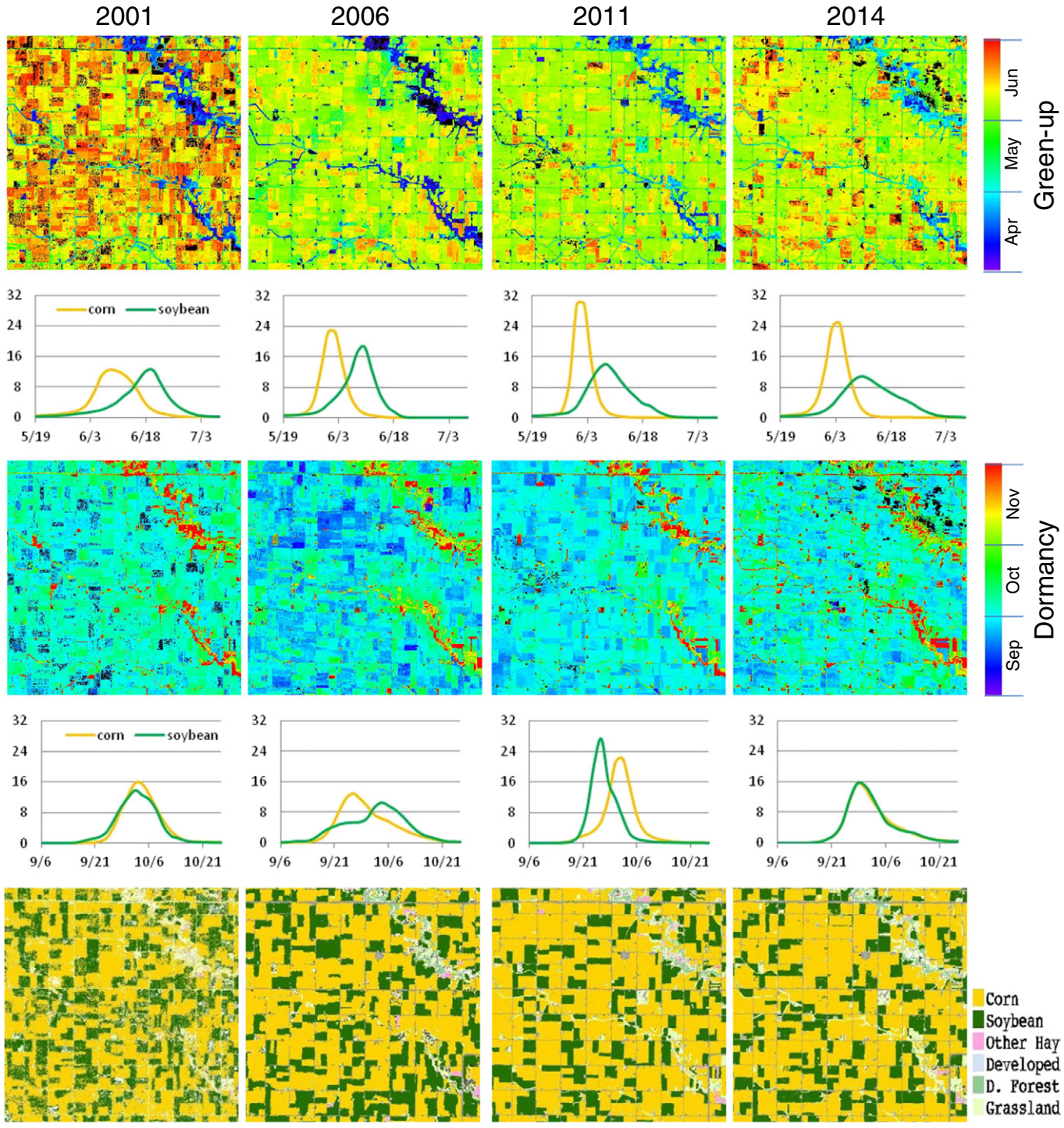

Fig. 8. Green-up and dormancy dates detected from the fused Landsat-MODIS data for 2001, 2006, 2011, and 2014. Top two rows show green-up dates (April to June) and histograms of green-up dates for corn (yellow) and soybean (green), the next two rows show dormancy dates (September to October) and histograms. Bottom row shows the CDL for the corresponding years in each column.

4.3.1. Comparison at tower sites

Fig. 9 shows the fitted NDVI curves from 2011 for corn and soybean pixels at the two South Fork flux tower sites, overlaid with the crop growth stages from NASS county-level CP reports. Also shown are daily NEE and GPP estimates derived from eddy covariance measurements during the growing season in 2011. The general correspondence in the time behavior of the NDVI and crop carbon uptake curves demonstrates that the NDVI time-series appears to be behaving reasonably in these two fields in relationship with the NASS CP stages.

In the early growing season, NDVI was around 0.2 in both fields during the county-average planting time. NDVI increased significantly after the NASS-reported emergence date, and close to the time net carbon uptake by the plant canopy is indicated in the flux measurements. Both NDVI and NEE/GPP reach maximum values around the same time – in the silking stage for corn and after pod-setting for soybean. NEE and GPP were almost linearly related to NDVI during the vegetative stages. The period of peak NDVI was shorter for soybean than for the corn site. Daily NEE/GPP entered decline around the time that NDVI

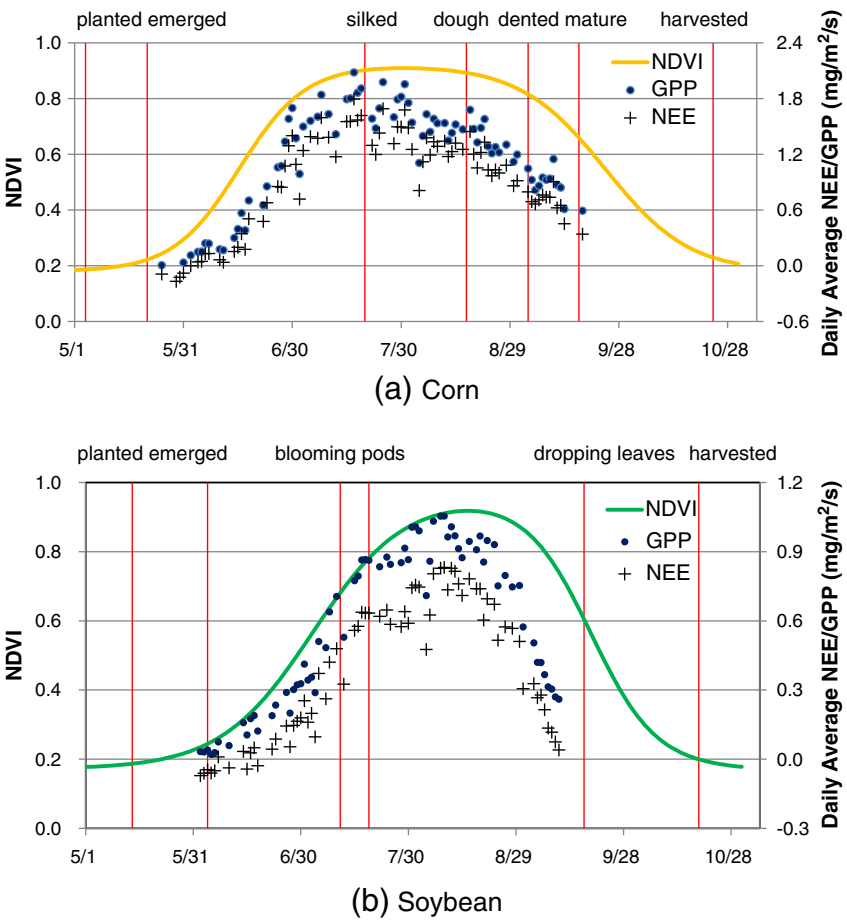

Fig. 9. NDVI curves for corn (a) and soybean (b) pixels compared to daily NEE and GPP (secondary axis, only measured during vegetative growing season) and crop growth stages from NASS county-level reports in 2011 (red vertical lines). Clear correspondences can be identified among time-series NDVI, NEE and GPP during crop vegetative stages at the Landsat pixel resolution.

started to decrease in each field, indicating a conversion of green to senesced biomass. NEE reached zero around the mature stage for corn and the leaf-drop stage for soybean. After the crops were harvested, NDVI values for both corn and soybean plots were restored to the pre-season values. Even though the crop growth stages were extracted from the NASS county level report and may not necessarily be expected to perfectly match conditions at the Fluxnet sites, Fig. 9 still shows clear correlations between NDVI time-series at 30-m resolution and specific crop growth stages observed on the ground.

4.3.2. Comparison at district level

As an example of performance at the district scale, Fig. 10 shows cumulative histograms of remotely sensed phenology metrics in comparison with growth stages reported by NASS for the "central Iowa" district in 2011. In this example, green-up dates retrieved from remote sensing data were consistently later than the reported emergence dates. The mid-season (peak NDVI) dates retrieved from the remote sensing data were between the silking and doughing stages for corn and close to the pod-setting stages for soybean. The dormancy (end of the season) dates were slightly ahead of the reported harvest time for both crops. The dormancy stage describes the date that the change of leaf colour or leaf drop were most significant. The dormancy stage for corn was detected after corn reached the mature stage when there was no green foliage present. For soybeans, the dormancy stage was detected after the leaf dropping stage. The fact that reported harvest dates occurred after the remotely sensed dormancy dates suggests that typical crop harvest dates could be predicted or estimated using remote sensing, keying off the retrieved dormancy dates. This could be useful both for management activities and for retrospective crop modeling efforts.

These temporal relationships between the remotely sensed phenology metrics and NASS reported crop stages were relatively stable across the years analyzed, when both the remote sensing and NASS reports were available (2010, 2011, 2013 and 2014). Fig. 11 shows scatter plots of median values (at 50% cumulative percentage) for green-up and dormancy dates for both corn and soybeans in comparison with NASS-reported emergence and harvest dates. The scatter plots show a strong linear correlation between the green-up dates and the emergence dates ($R^2 = 0.83$) for both corn and soybeans. Green-up dates were later than the emergence dates as noted above. Green-up dates at the pixel level were compared to the field observations at a corn site (41.644N, 94.154W) and a soybean site (41.644N, 94.145W) in Dallas County, Iowa in 2010 (see Section 2.6). The remotely sensed green-up dates at were on May 31 and June 13 for the corn and soybean sites, respectively. On these dates, the field observations indicate that both crops were primarily in the V3 stage, with plants exhibit 2–4 leaves. The V3 stage normally occurs 2–3 weeks after emergence.

A comparison of dormancy and harvest dates reveals somewhat different relationships for corn and soybeans. Corn was harvested within 2–3 weeks and soybeans within 1–2 weeks after dormancy dates were detected via remote sensing, as indicated by rapid changes in NDVI (green vegetation) during the end of the season. The 2010 field observations in Dallas County, Iowa also revealed a similar finding at the Landsat pixel resolution. For the corn site, the mature stage was first reported on September 11, the dormancy date was detected on September 17 and the harvest date was after September 25 (last

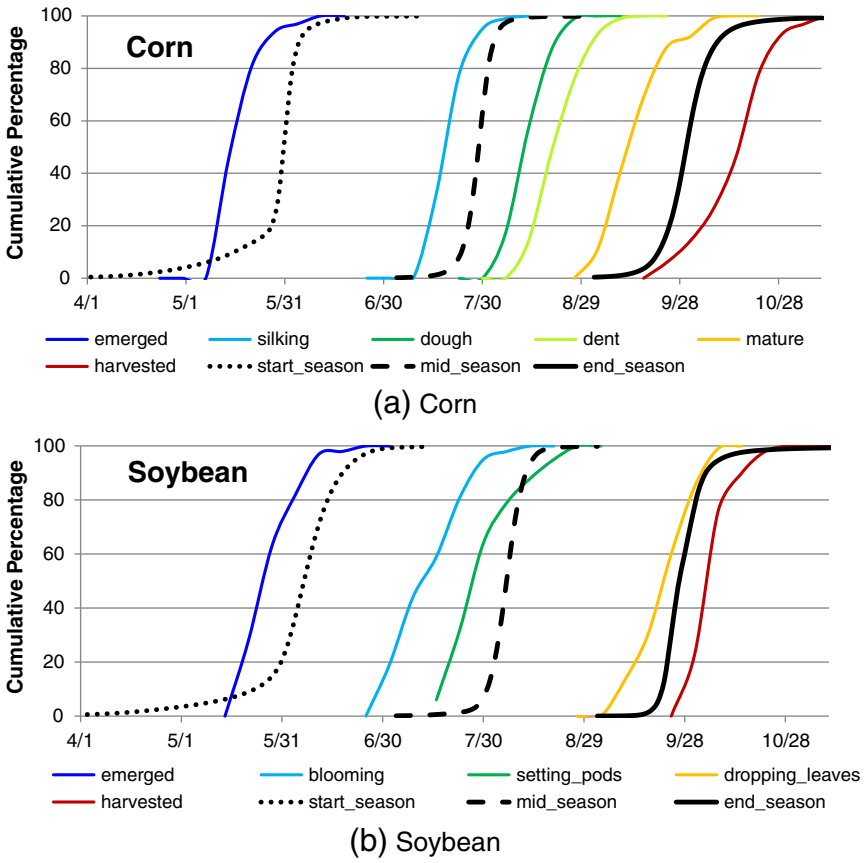

Fig. 10. Phenology dates detected from the fused Landsat-MODIS data (colored curves) and crop growth stages reported in the NASS CP reports (dotted, dashed and solid black lines) at district level for central Iowa in 2011.

reported mature date). For the soybean site, the mature stage was first reached on September 17, the dormancy date was detected on September 23 and the harvest date was after September 26 (last reported mature date). Soybeans need to be harvested within a short period of time after leaves drop to avoid pre-harvest loss. This may be a reason why harvest dates for soybeans were closer to the dormancy dates from remote sensing.

In Fig. 12, these district-level comparisons are extended over the full set of years analyzed. For better illustration, the range on the two y-axes for each plot has been adjusted to optimize alignment, using the linear relationships between crop phenology and growth stages shown in Fig. 11. Even though the NASS CP reports were summarized based on sparsely distributed field surveys, a general agreement of trend between remote sensing phenology and the NASS CP data can be observed (see also Fig. 11). The remote sensing phenology captures the later green-up in 2013 observed by NASS reporters on the ground for both corn and soybeans. The offset in green-up between corn and soybean detected by the remote sensing is relatively uniform back through years prior to the NASS CP reporting era (before 2011). The late green-up dates in 2007 were likely due to wet conditions in early spring, as farmers were forced to wait for drier weather (NASS Bulletin, 2007). While corn green-up always preceded soybean, relative remote sensing dormancy dates for corn and soybean varied from year to year (also illustrated in Fig. 8). Even though harvesting date for individual fields depends on numerous non-biotic factors, including human resources, weather and marketing decisions, there are general correlations

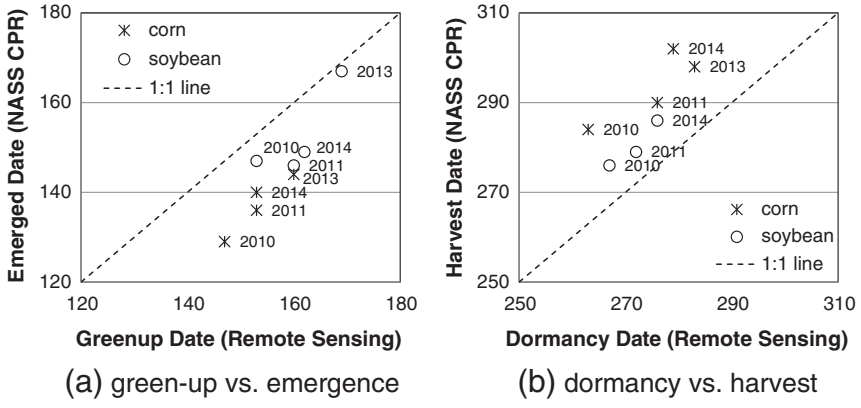

Fig. 11. Crop phenology (green-up and dormancy dates) detected using the fused Landsat and MODIS data compared to the crop progress stages (emergence and harvest dates) reported in the NASS CP reports in central Iowa (district level) for 2010, 2011, 2013 and 2014 (soybean harvest dates in 2013 were not available for central Iowa in the report).

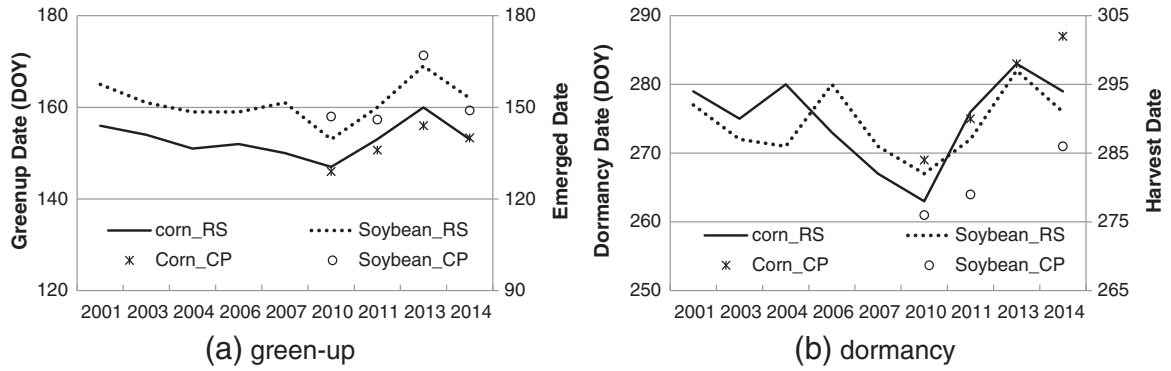

Fig. 12. Crop phenology (primary axis) detected using the fused Landsat-MODIS remote sensing data (RS) in processed years from 2001 to 2014 overlaid with the crop growth stages (secondary axis, difference range of dates) from the district-level NASS CP reports for central Iowa (available 2010 to 2014).

between remote sensing dormancy dates and observed harvest dates for corn and soybeans. The trend observed in recent years (2010–2014) demonstrates a potential to forecast "expected" harvest dates for corn and soybeans after dormancy is detected via remote sensing. In 2014, the soybean and corn harvests were 1–2 weeks behind normal schedule due to a rain delay. As shown in Fig. 11, the harvest dates for individual fields may be forecasted 1–3 weeks ahead of harvest operation.

4.3.3. Comparison at county level

The county-level information provided by NASS for 2010 and 2011 allows an assessment of fused NDVI time-series performance at finer (sub-district) scales of spatial aggregation. Fig. 13 compares remote sensing and NASS crop growth stages for corn and soybean from 17 individual counties that were completely covered by the processed Landsat scene (Fig. 1). Counties are not identified by name to comply with the NASS privacy agreement. The relative delay in detected green-up date with respect to NASS reported emergence dates (Fig. 13a and d) is similar to that inferred at the field and district levels (Figs. 7 and 10). The median delay over these counties was 17 days for corn and 9 days for soybean. Green-up was detected close to the V3 physiological growth stage (approximately three leaves apparent), and occurred about 6–7 days earlier for corn than for soybean for both years. The dormancy dates detected for corn were between the reported

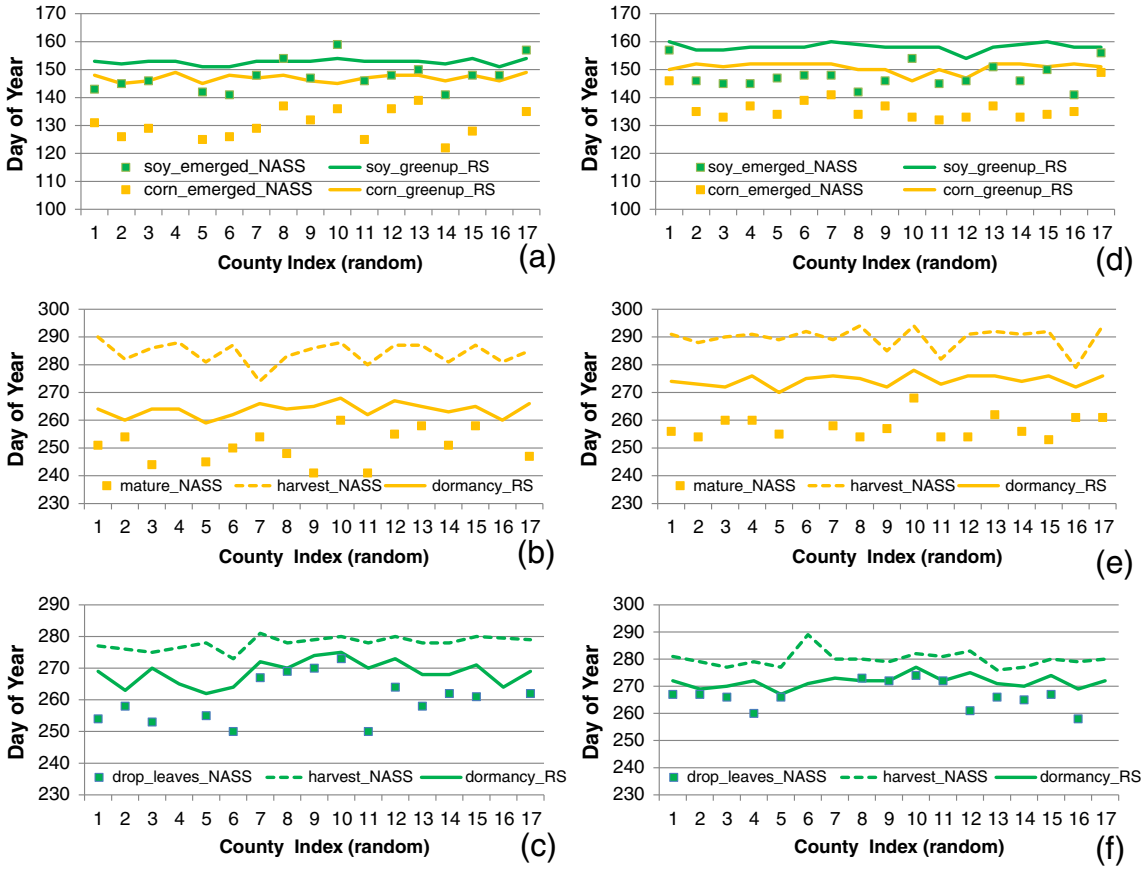

Fig. 13. Crop growth stages reported from 17 counties (county level, x-axis used random index) and crop phenology extracted from remote sensing in 2010 (left) and 2011 (right). The emergence and green-up dates for corn and soybeans are compared in (a) and (d); the mature and harvest stages are compared to the dormancy date for corn in (b) and (e); the leaf-drop and harvest stages for soybeans are compared to the dormancy dates in (c) and (f).

maturation and harvest dates (Fig. 13b and e). The dormancy dates for soybean were between the reported leaf-drop and harvest dates (Fig. 13c and f). Dormancy dates of soybeans in some counties were very close to the leaf-drop stage, because the leaves at the very top of the canopy may still be green at this stage (definition in Section 2.3). The median number of days between dormancy and harvest date for the 17 counties was 14–21 days and 6–8 days for corn and soybeans, respectively, which agrees with the statistics at the district level from 2010 to 201 (Section 4.3.2). The relative consistency between the remote sensing and ground observer derived metrics demonstrated here suggest a reliable relationship between crop growth stage and remote sensing phenology could be established for operational applications.

5. Discussion

The results presented in Section 4 show that crop phenology at field scales can be reasonably deduced by combining VI data from Landsat and MODIS. However, mapping of crop phenology at field scale is still challenging due primarily to the lack of clear observations available at the Landsat pixel resolution. Several limitations and opportunities for the proposed methodologies are discussed further below, associated with both the data fusion and the phenology extraction components of the integrated system.

5.1. Data fusion limitations and opportunities

5.1.1. Landsat temporal frequency

A good seasonal distribution of clear Landsat-scale images is required for producing high quality data fusion results. In particular, Landsat imagery from the early growing season is critical since it provides remote sensing signals that can be used to separate different crop types. This is a typically rainy/cloudy period in the Corn Belt, and therefore in some years it is difficult to capture this early part of the season adequately with Landsat alone.

The recently launched Sentinel-2 satellite provides additional global Landsat-resolution imagery at no cost to users, which could be combined with Landsat data for mapping crop phenology. However, consistency of new data sources needs to be assessed. Differences in surface reflectance or NDVI may be caused by different sensor characteristics (e.g. spectral bandwidth) or data processing techniques (calibration and atmosphere correction). A normalization approach may be considered to convert surface reflectance from Landsat-resolution sensors to MODIS-like surface reflectance using MODIS NBAR data as a reference, as described in Gao et al. (2010). A relatively consistent time-series data from different sensors could be more important than absolute inter-sensor calibration.

5.1.2. Landsat-MODIS mismatch

Terra MODIS has a similar orbit to Landsat 7 ETM + and thus MODIS and ETM + images match better than do other MODIS-Landsat combinations. However, ETM + imagery after May 2003 is not as useful for data fusion due to the SLC-off gaps. Landsat 8 OLI acquisition dates are 8 days apart from Landsat 7, and Terra MODIS images are always acquired from off-nadir views at the Landsat 8 overpass time. In this study, we have corrected MODIS daily 250 m directional surface reflectance to daily NBAR (daily NBAR products at 500 m resolution are now routinely available in the MODIS Collection 6 reprocessing). However, off-nadir views also cause a reduction of spatial resolution in the MODIS image and thus the MODIS data quality at off-nadir is lower when comparing to nadir view (Tan et al., 2006). While we could exclude MODIS observations at large off-nadir views, this would limit the temporal frequency of available MODIS imagery. A possible solution is to use Aqua MODIS data to pair with Landsat 8 OLI imagery. The Aqua MODIS imagery is acquired at around 1:30 pm but has a smaller view zenith angle on Landsat 8 acquisition dates. The Aqua MODIS imagery can be corrected to daily NBAR using the solar angles at the Landsat 8 overpass time. Since Aqua MODIS and Landsat 8 OLI images are acquired at different times, cloud coverage could be different in Landsat and MODIS images, which may limit their uses in the data fusion process. Using a composite image generated from Aqua and Terra MODIS data may be another solution. As MODIS sensors are aging, other coarse-resolution imagery such as the Visible Infrared Imaging Radiometer Suite (VIIRS) may be used. The VIIRS sensor has a better spatial resolution at off-nadir views, which could make it a good candidate for combination with (or replacement of) MODIS.

5.1.3. Computational efficiency

The STARFM program has recently been significantly improved in terms of computational efficiency – this is of particular relevance to end-users using the original version of the system (V1.1). In the original version, the entire STARFM algorithm had to be rerun for each prediction date. In the current version, predictions for multiple MODIS dates that use the same Landsat-MODIS input pair are combined into a single run (V1.2; Gao et al., 2015 – available freely online). Therefore, the search time for spectrally similar pixels in the moving window (the most time-consuming part) is greatly reduced. Testing demonstrated that the processing time for 30 predictions using a single input pair reduced from 540 min to 78 min between V1.1 and 1.2, using a single CPU (Intel Xeon 3.07 GHz). In addition, parallel computing options implemented in this version further reduced computing time to about 17 min for 30 predictions (~31 times faster than V1.1). These improvements allow us to run the data fusion algorithm efficiently over an entire Landsat scene on a personal Linux system. It took about a week on our computing system to download and process Landsat and MODIS data for a single Landsat scene covering a whole year. However, processing data over large areas (e.g. entire state or country) for multiple years is still a challenge. High performance computing resources are needed for a large-area applications.

5.2. Linking remote sensing with physiological growth stages

This study explored and identified relationships that exist between phenological metrics that can be derived from remote sensing and physiological stages of crop growth observed on the ground. The latter information is directly usable in many applications, from yield prediction to farm management. The next phase of this research will involve determining robust yet simple methods for linking the remote sensing and physiological stages, to support crop progress monitoring over large areas.

While a calendar date offset appeared to reasonably capture much of the variability between remote sensing and physiological stages observed over central Iowa during the limited time period studied here, a degree day model for connecting these stages may be more robust for large-area monitoring. Particularly in the spring, the period between planting/emergence and the V3 stage captured as “green-up” in the remote sensing data will largely be governed by degree day accumulations within the Corn Belt.

Practically speaking, there is great potential utility for large area green-up maps, even though the green-up signal lags actual planting and emergence dates. Planting/emergence could be backcasted from green-up and used to check/adjust ground-based reports, which are typically based on limited sparsely distributed samples. Planting/emergence is a critical variable in crop simulations, used to forecast the impacts of weather, disease and pest on at-harvest yield, but it is very difficult to obtain accurate planting and emergence dates from ground reports (Jones et al., 2003; Sacks et al., 2010). Remote-sensing based backcasts may help to address these critical data issues in spatially distributed crop modeling efforts.

Harvest typically occurs after the remotely sensed dormancy period, and therefore could be forecasted. Remote sensing maps of dormancy, developed in real-time, could be used for harvest planning to reduce

pre-harvest loss, especially for soybeans since they are fragile during harvest time.

This study used NDVI time-series to detect green-up and senescent stages when NDVI has not reached the saturation value. For crop stages during peak green season, other vegetation indices such as the Enhanced Vegetation Index (EVI) or two-band EVI (EVI2) may be more appropriate. Crop phenology detected using different vegetation indices may result in different phenological dates, and the relationships between phenology and crop growth stages may vary with index. These effects need to be further investigated.

Some crop growth stages may not be detectable from remote sensing signals directly. These stages may be determined using other ancillary information such as crop calendars and growing degree days. The two-step filtering approach of Sakamoto et al. (2010, 2011) uses a predefined shape model describing characteristic crop growth patterns as a priori information, fit to vegetation index time-series to capture dynamic conditions for a given growing season. The fitted shape model is then used to extract detailed phenological growth stages. Sakamoto et al. tested the approach using MODIS-derived vegetation index data at 250-m spatial resolution and daily timesteps. This approach could be extended to field scale using daily 30-m resolution fused Landsat-MODIS surface reflectance data to map growth stages at finer granularity than those investigated here.

Application of these methods in real-time is another area that requires additional research. Operationally, crop growth stages and conditions need to be reported weekly throughout the current growing season. The phenology programs used in this paper were not designed to map within-season crop phenology using partial years of data. However, the growth-shape model approach of Sakamoto et al. (2010, 2011) may be adaptable for real-time field-scale applications using fused Landsat-MODIS timeseries.

6. Conclusion

The study presented here addressed three main objectives; the evaluation of fused Landsat-MODIS reflectance and the derived vegetation index time-series, the use of these time-series to derive remote sensing metrics of crop phenology, and the investigation of connections between remote sensing metrics and physiological crop growth stages reported at field, county and district scales. The study combined the STARFM data fusion system with the MODIS time-series approach for phenology extraction to produce maps of crop progress at 30-m resolution across an intensively cropped area in central Iowa.

The STARFM approach was used to produce multi-year daily 30-m surface reflectance and NDVI time-series which captured spatial and seasonal variability between the corn, soybean and forested vegetation classes that characterize this region. Biases between fused and observed Normalized Difference Vegetation Index (NDVI) were between −0.011 to 0.028 and mean absolute differences were <0.083 for all years from 2001 to 2014. These biases are due in part to sensor, waveband, and view angle differences between Landsat and MODIS acquisitions, and it was demonstrated that it is important to characterize these biases to fully understand performance of the fusion output.

Using time-series of 30-m resolution NDVI maps derived from Landsat-MODIS data fusion, crop phenological metrics were extracted using two established phenology programs (MODIS and TIMESAT). While both approaches generated comparable metrics, the MODIS curvature approach was deemed most practical for operational applications because it does not necessitate specification of pre-defined thresholds, as required by the TIMESAT approach. Comparison with NASS crop progress reports generated at the county and district levels shows that the remotely sensed crop green-up dates were later than the reported emergence dates for all years, close to the V3 stage where 2–4 leaves have developed. At this stage, rapid changes in satellite-derived NDVI signal were most apparent. While this remotely sensible stage proceeds emergence, which is the date plants are first visible from the ground, a high correlation between the two dates was found over the period 2010–2014, when the NASS crop progress reports at district level were available. This suggests utility for robustly backcasting emergence from remote sensing, e.g. as input to crop simulation models. The detected dormancy dates were 2–3 weeks ahead of harvest time for corn and about 1–2 weeks ahead for soybeans. The harvest times for individual fields may be predicted 1–3 weeks ahead using remote sensing data, which could help to manage crop harvest at field level to reduce pre-harvest loss.

This study demonstrated that time-series data from multiple remote sensing sources can be effectively integrated and used to detect major crop physiological stages at the field scale. At 30-m resolution, the phenology for corn and soybean crops can be clearly separated and quantified for field sizes typical in the United States. This capability has applications in farmland management and yield prediction. However, routine mapping of crop growth stages within the season is still challenging due to the fact that only a partial year of data is available for near real-time mapping. Real-time applications will require an appropriate phenology approach and frequent clear-sky remote sensing imagery. Satellite image data fusion can play a significant role in achieving this goal.

Acknowledgement

This work was supported by the NASA Science of Terra and Aqua program (NNH13ZDA001N-TERAQ) and the US Geological Survey (USGS) Landsat Science Team program. The collection of field biophysical data was funded by NASA grant NNX09AO14G. USDA is an equal opportunity provider and employer.

References

Boryan, C., Yang, Z., Mueller, R., Craig, M., 2011. Monitoring US agriculture: the US Department of Agriculture, National Agricultural Statistics Service, Cropland Data Layer Program. Geocarto Int. 26 (5), 341–358.

Feng, M., Sexton, J., Huang, C., Masek, J., Vermote, E., Gao, F., Narasimhan, R., Channan, S., Wolfe, R., Townshend, J., 2013. Global surface reflectance products from Landsat: assessment using coincident MODIS observations. Remote Sens. Environ. 134, 276–293.

Friedl, M.A., McIver, D.K., Hodges, J.C.F., et al., 2002. Global land cover from MODIS: Algorithms and early results. Remote Sens. Environ. 83, 287–302.

Gao, F., Masek, J., Schwaller, M., Hall, F., 2006. On the blending of the Landsat and MODIS surface reflectance: predict daily Landsat surface reflectance. IEEE Trans. Geosci. Remote Sens. 44 (8), 2207–2218.

Gao, F., Morisette, J.T., Wolfe, R.E., Ederer, G., Pedelty, J., Masuoka, E., Myneni, R., Tan, B., Nightingale, J., 2008. An algorithm to produce temporally and spatially continuous MODIS LAI time series. IEEE Geosci. Remote Sens. Lett. 5 (1), 60–64.

Gao, F., Masek, J., Wolfe, R., Huang, C., 2010. Building consistent medium resolution satellite data set using moderate resolution imaging spectroradiometer products as reference. J. Appl. Remote. Sens. 4:043526. http://dx.doi.org/10.1117/1.3430002.

Gao, F., Hilker, T., Zhu, X., Anderson, M., Masek, J., Wang, P., Yang, Y., 2015. Fusing Landsat and MODIS data for vegetation monitoring. IEEE Geosci. Remote Sens. Mag. 3 (3), 47–60.

Goring, D.G., Nikora, V.I., 2002. Despiking acoustic doppler velocimeter data. J. Hydrol. Eng. 128, 117–126.

Hilker, T., Wulder, M.A., Coops, N.C., Linke, J., McDermid, G., Masek, J.G., Gao, F., White, J.C., 2009. A new data fusion model for high spatial- and temporal-resolution mapping of forest disturbance based on Landsat and MODIS. Remote Sens. Environ. 113 (8), 1613–1627.

Jones, J.W., Hoogenboom, G., Porter, C.H., Boote, K.J., Batchelor, W.D., Hunt, L.A., Wilkens, P.W., Singh, U., Gijsman, A.J., Ritchie, J.T., 2003. DSSAT cropping system model. Eur. J. Agron. 18, 235–265.

Jonsson, P., Eklundh, L., 2004. TIMESAT - a program for analysing time-series of satellite sensor data. Comput. Geosci. 30, 833–845.

Kucharik, C.J., 2006. A multidecadal trend of earlier corn planting in the central USA. Agron. J. 98 (6), 1544–1550.

Liang, L., Schwartz, M., Wang, Z., Gao, F., Schaaf, C., Tan, B., Morisette, J., Zhang, X., 2014. A cross comparison of spatiotemporally enhanced springtime phenological measurements from satellites and ground in a northern U.S. mixed forest. IEEE Trans. Geosci. Remote Sens. 52 (12):7513–7526. http://dx.doi.org/10.1109/TGRS.2014.2313558.

Lehecka, G.V., 2014. The value of USDA crop progress and condition information: reactions of corn and soybeans futures markets. J. Agric. Resour. Econ. 39 (1), 88–105.

Loveland, T.R., Dwyer, J.L., 2012. Landsat-building a strong future. Remote Sens. Environ. 122, 22–29.

Masek, J.G., Vermote, E.F., Saleous, N.E., et al., 2006. A Landsat surface reflectance data set for North America, 1990–2000. IEEE Geosci. Remote Sens. Lett. 3 (1), 69–72.

NASS CPR, 2015. http://www.nass.usda.gov/Publications/National_Crop_Progress/ (last accessed November 30, 2015).
NASS Bulletin, 2007. http://www.nass.usda.gov/Statistics_by_State/Iowa/Publications/Annual_Statistical_Bulletin/2008/45_08.pdf (last accessed November 30, 2015).
NASS CDL, 2015. http://www.nass.usda.gov/Research_and_Science/Cropland/SARS1a.php (last accessed November 30, 2015).
NASS Field Crops, 1997. Usual Planting and Harvesting Dates. http://usda.mannlib.cornell.edu/usda/current/planting/planting-10-29-2010.pdf (last accessed November 30, 2015).
NASS Field Crops, 2010. Usual Planting and Harvesting Dates. http://usda.mannlib.cornell.edu/usda/nass/planting//1990s/1997/planting-12-05-1997.pdf (last accessed November 30, 2015).
NASS Terms, 2015. http://www.nass.usda.gov/Publications/National_Crop_Progress/Terms_and_Definitions/ (last accessed November 30, 2015).
Reed, B.C., Brown, J.F., Vander Zee, D., Loveland, T.R., Merchant, J.W., Ohlen, D.O., 1994. Measuring phenological variability from satellite imagery. J. Veg. Sci. 5, 703–714.
Ren, J., Campbell, J.B., Shao, Y., 2014. Agricultural land use changes, 2001–2012, southeastern Iowa, using Landsat 4 &5 TM imagery. ASPRS 2014 Annual Conference Proceedings, Louisville, Kentucky, USA, March 23–28, 2014 http://www.asprs.org/a/publications/proceedings/Louisville2014/Ren.pdf (last accessed November 30, 2015).
Roy, D.P., Wulder, M.A., Loveland, T.R., et al., 2014. Landsat-8: science and product vision for terrestrial global change research. Remote Sens. Environ. 145, 154–172.
Sacks, W.J., Deryng, D., Foley, J.A., Ramankutty, N., 2010. Crop planting dates: an analysis of global patterns. Glob. Ecol. Biogeogr. 9, 607–620.
Sakamoto, T., Wardlow, B.D., Gitelson, A.A., Verma, S.B., Suyker, A.E., Arkebauer, T.J., 2010. A two-step filtering approach for detecting maize and soybean phenology with time-series MODIS data. Remote Sens. Environ. 114, 2146–2159.
Sakamoto, T., Wardlow, B.D., Gitelson, A.A., 2011. Detecting spatiotemporal changes of corn developmental stages in the US Corn Belt using MODIS WDRVI data. IEEE Trans. Geosci. Remote Sens. 49, 1926–1936.
Sakamoto, T., Gitelson, A.A., Arkebauer, T.J., 2013. MODIS-based corn grain yield estimation model incorporating crop phenology information. Remote Sens. Environ. 131, 215–231.
Schaaf, C.L.B., Gao, F., Strahler, A.H., et al., 2002. First operational BRDF, albedo and nadir reflectance products from MODIS. Remote Sens. Environ. 83, 135–148.
Schaaf, C.L.B., Liu, J., Gao, F., Strahler, A.H., 2011. MODIS Albedo and reflectance anisotropy products from Aqua and Terra. In: Ramachandran, B., Justice, C., Abrams, M. (Eds.), Land Remote Sensing and Global Environmental Change: NASA's Earth Observing System and the Science of ASTER and MODIS, Remote Sensing and Digital Image Processing Series vol. 11. Springer-Cerlag (873 pp).
Tan, B., Woodcock, C.E., Hu, J., et al., 2006. The impact of gridding artifacts on the local spatial properties of MODIS data: implications for validation, compositing, and band-to-band registration across resolutions. Remote Sens. Environ. 105, 98–114.
Vermote, E.F., El Saleous, N.Z., Justice, C.O., 2002. Atmospheric correction of MODIS data in the visible to middle infrared: first results. Remote Sens. Environ. 83, 97–111.
Walker, J., Beurs, K.M., Wynne, R.H., Gao, F., 2012. Evaluation of Landsat and MODIS data fusion products for analysis of dryland forest phenology. Remote Sens. Environ. 117: 381–393. http://dx.doi.org/10.1016/j.rse.2011.10.014.
Walthall, C.L., Hatfield, J., Backlund, P., et al., 2012. Climate Change and Agriculture in the United States: Effects and Adaptation. USDA Technical Bulletin 1935. Washington, DC (186 pages).
Wang, P., Gao, F., Masek, J., 2014. Operational data fusion framework for building frequent Landsat-like images. IEEE Trans. Geosci. Remote Sens. 52 (1), 7353–7365.
Woodcock, C.E., Allen, R., Anderson, M., Belward, A., Bindschadler, R., Cohen, W.B., Gao, F., Goward, S.N., Helder, D., Helmer, E., Nemani, R., Oreopoulos, L., Schott, J., Thenkabail, P.S., Vermote, E.F., Vogelmann, J., Wulder, M.A., Wynne, R., 2008. Free access to Landsat imagery. Science 320, 1011.
Xiao, X., Hollinger, D., Aber, J., Goltz, M., Davidson, E.A., Zhang, Q., Moore, B., 2004. Satellite-based modeling of gross primary production in an evergreen needleleaf forest. Remote Sens. Environ. 89, 519–534.
Zhang, X., Friedl, M.A., Schaaf, C.B., Strahler, A.H., Hodges, J.C.F., Gao, F., Reed, B.C., 2003. Monitoring vegetation phenology using MODIS. Remote Sens. Environ. 84 (3), 471–475.
Zhang, X., 2015. Reconstruction of a complete global time series of daily vegetation index trajectory from long-term AVHRR data. Remote Sens. Environ. 156, 457–472.
Zhao, H., Yang, Z., Di, L., Li, L., Zhu, H., 2009. Crop phenology date estimation based on NDVI derived from the reconstructed MODIS daily surface reflectance data. 2009 17th International Conference on Geoinformatics http://dx.doi.org/10.1109/GEOINFORMATICS.2009.5293522 .
Zhao, H., Yang, Z., Di, L., Pei, Z., 2012. Evaluation of temporal resolution effect in remote sensing based crop phenology detection studies. Computer and Computing Technologies in Agriculture V the series IFIP Advances in Information and Communication Technology. 369, pp. 135–150.
Zhu, X., Chen, J., Gao, F., Masek, J., 2010. An enhanced spatial and temporal adaptive reflectance fusion model for complex heterogeneous regions. Remote Sens. Environ. 114, 2610–2623.
Zhu, Z., Woodcock, C.E., 2012. Object-based cloud and cloud shadow detection in Landsat imagery. Remote Sens. Environ. 118, 83–94.
Zhu, Z., Woodcock, C.E., 2015. Improvement and expansion of the Fmask algorithm: cloud, cloud shadow, and snow detection for Landsats 4–7, 8, and sentinel 2 images. Remote Sens. Environ. 159, 269–277.